Supplementary Materials for

Engineering micromechanics of soft porous crystals for negative gas adsorption

Simon Krause[a,b]*, Jack D. Evans[a]*, Volodymyr Bon[a], Irena Senkovska[a], Sebastian Ehrling[a], Paul Iacomi[c,e], Daniel M. Többens[d], Dirk Wallacher[d], Manfred S. Weiss[d], Bin Zheng[e,f], Pascal G. Yot[e], Guillaume Maurin[e], Philip L. Llewellyn[c], François-Xavier Coudert[g], Stefan Kaskel[a]*

a) Faculty of Chemistry and Food Chemistry, TU Dresden, Bergstrasse 66, 01069, Dresden, Germany

b) Centre for Systems Chemistry, Stratingh Institute for Chemistry, University of Groningen, Nijenborgh 4, 9747 AG Groningen, The Netherlands

c) Aix-Marseille Univ., CNRS, MADIREL (UMR 7246), 13013, Marseille, France

d) Helmholtz-Zentrum Berlin für Materialien und Energie, Hahn-Meitner-Platz 1, 14109, Berlin, Germany

e) ICGM, Univ. Montpellier, CNRS, ENSCM, Montpellier, France

f) School of Materials Science and Engineering, Xi'an University of Science and Technology, Xi'an 710054, PR China

g) Chimie ParisTech, PSL University, CNRS, Institut de Recherche de Chimie Paris, 75005, Paris, France

Correspondence to:

Simon Krause: simon.krause@rug.nl

Jack D. Evans: jack.evans@tu-dresden.de

Stefan Kaskel: Stefan.kaskel@tu-dresden.de

Table of contents

1 Instruments and methods

The description of instruments and methods has been previously published by our group in reference [1] and is a literal adaption.

Solution/liquid-state NMR

Nuclear magnetic resonance (NMR) spectra were acquired on a BRUKER Avance III 500 spectrometer (500.13/600.16 MHz and 125.77/150.91 MHz for ^{1}H and ^{13}C respectively) and/or on a VARIAN Mercury (300 MHz, 282 MHz and 75.5 MHz for ^{1}H and ^{13}C, respectively). All ^{1}H and ^{13}C NMR spectra are reported in parts per million (ppm) downfield of TMS and were measured relative to the residual signals of the solvents at 7.26 ppm ($CHCl_3$) or 2.54 ppm (DMSO). Data for ^{1}H NMR spectra are described as following: chemical shift (δ (ppm)), multiplicity (s, singlet; d, doublet; t, triplet; q, quartet; m, multiplet; br, broad signal), coupling constant *J* (Hz), integration corresponding to amount of C or CH. Data for ^{13}C NMR spectra are described in terms of chemical shift (δ (ppm)) and functionality were derived from DEPT spectra.

Mass spectrometry

Matrix-assisted laser desorption/ionization (MALDI) time of flight (TOF) mass spectrometry analysis was performed on a BRUKER Autoflex Speed MALDI TOF MS using dithranol as matrix. Atmospheric-pressure solid analysis probe (ASAP) mass spectrometry was performed on an ADVION expression LCMS with an APCI ion source.

Elemental analysis

Elemental analysis was carried out on a VARIO MICRO-cube Elemental Analyzer by Elementar Analysatorsysteme GmbH in CHNS modus. The composition was determined as the average of three individual measurements on three individually prepared samples.

DRIFT Spectroscopy

Diffuse reflectance infrared Fourier transform (DRIFT) spectroscopy was performed on a BRUKER VERTEX 70 with a SPECAC Golden Gate DRIFT setup. Prior to the measurement 2 mg of sample were mixed with 10-15 mg dry KBr in a mortar and pressed in the DRIFT-cell. Assignments of peaks in wavenumber ν (cm^{-1}) were categorized by strong (s), medium (m), weak (w).

Thermogravimetric analysis

Thermal analysis (TGA) was carried out in synthetic dry air using a NETZSCH STA 409 thermal analyser at a heating rate of 5 K min^{-1}. Air sensitive MOF samples were prepared in an Ar-filled glovebox and inserted in the instrument with little exposure to ambient conditions.

X-Ray Diffraction

Powder X-ray diffraction (PXRD) patterns were collected in transmission geometry with a STOE STADI P diffractometer operated at 40 kV and 30 mA with monochromatic Cu-$K\alpha_1$ (λ = 0.15405 nm) radiation, a scan speed of 30 - 15 s/step and a detector step size of 2Θ = 0.1 – 2 °. The samples were placed between non-diffracting adhesive tape or in a glass capillary. “As made” samples were analysed while suspended in DMF. Desolvated samples were prepared under inert atmosphere. Theoretical PXRD patterns were calculated on the basis of crystal structures using Mercury 3.9 software package.

SEM analysis of crystal size and morphology

Scanning electron microscopy (SEM) images of DUT-49 were taken with secondary electrons in a HITACHI SU8020 microscope using 1.0 kV acceleration voltage and 10.8 mm working distance. The powdered samples were prepared on a sticky carbon sample holder. To avoid degradation upon exposure to air, the samples were prepared under argon atmosphere. For each sample a series of images was recorded at different magnifications and for each sample three different spots on the sample holder were investigated. The crystal size refers to the edge length of the cubic crystals as they are the easiest to measure. The analysis of the SEM images was performed with ImageJ Software package.[2] Values for mean crystal size, as well as relative standard deviation (RSD) were obtained by using the ImageJ Analyse-Distribution function.

2 Materials and Ligand synthesis

For the synthesis and characterisation the following commercial chemicals were used: 2,7-Dibromopyrene (CAS:102587-98-4, >97%, TCI), 4,4′-Diiodo-2,2′-dimethyl-1,1′-biphenyl (CAS:69571-02-4, 97%, Sigma Aldrich), 9,10-Hydrophenanthrene (Cas: 776-35-2, 99%, ABCR), Bis(4-Bromophenyl)acetylene (2789-89-1, >98%, TCI), Copper(II) nitrate trihydrate (10031-43-3, 98%, Sigma Aldrich), Dibromo-p-xylene (623-24-5, 98%, Sigma Aldrich), 4,4'-Dibromo-trans-stilbene (CAS: 18869-30-2, 99%, TCI), Copper(I) iodide (CAS: 7681-65-4, 99%, Riedel-de Haen).

Synthesis procedures

General procedures for the synthesis of the ligands described below were previously published by our group[1] The Synthesis is based on *n*-butyl ester 1 which can be obtained in a 5 step synthesis from 9*H*-carbazole following procedures published in reference [1, 3].

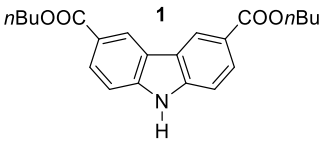

Supplementary Figure 1. Chemical structure of *n*-butyl ester **1**.The general synthesis of the ligands is based on Ullmann coupling of the ester **1** with different iodides and bromines. The following procedures which were previously published in reference [1] were used:

Ullmann coupling with iodides

This procedure is based on synthesis previously used for carbazole based ligands[4]. A Schlenk flask was charged with indicated amounts of ester **1**, the corresponding iodine, potassium carbonate, copper (I) iodide, and *L*-proline under inert atmosphere. To the mixture indicated amounts of degassed DMSO or DMF were given and Ar was bubbled through the suspension for 30 min. The reaction mixture was stirred at 90 – 120 °C for 24 h to 10 d and the reaction was cooled down to room temperature. The suspension was quenched with diluted (< 0.02 M) Hydrochloric acid and extracted with chloroform. He organic phases were collected, dried over $MgSO_4$, and the solvent removed in vacuum. The crude product was purified by flash column chromatography using indicated mixtures of chloroform, DCM, *iso*-hexane and ethyl acetate. Corresponding amounts of the chemicals added and used for the synthesis and purification are provided for each coupling product.

Ullmann coupling with bromides

This procedure is based on synthesis previously used for carbazole based ligands[5]. A Schlenk flask was charged with indicated amounts of ester **1** the corresponding bromide, potassium carbonate, copper (I) iodide, and *N,N'*-dimethylethylenediamine under inert atmosphere. To the mixture indicated amounts of degassed anhydrous 1,4-dioxane were given and Ar was bubbled through the suspension for 30 min. The reaction mixture was stirred at 80 – 110 °C for 24 h to 12 d and the reaction was cooled down to room temperature. The solvent was removed in vacuum and the obtained powder was dissolved in chloroform and extracted with diluted (< 0.02 M) hydrochloric acid. He organic phases were collected, dried over $MgSO_4$, and the solvent removed in vacuum. The crude product was purified by flash column chromatography using indicated mixtures of chloroform, DCM, *iso*-hexane and ethyl acetate. Corresponding amounts of the chemicals added and used for the synthesis and purification, reaction times and temperatures are provided for each coupling product.

General procedure for ester hydrolysis

To hydrolyse the ester groups the corresponding coupling products were dissolved in indicated volumes of THF, methanol, and water at 85 °C. To the solution potassium hydroxide was added and the mixture was stirred at 85 °C for 12 h– 5 d. In case a precipitation formed from the previous clear solution (most

likely the potassium salt of the hydrolysed ester which is insoluble in THF) small amounts of water were added until a clear solution formed again. After the indicated reaction time the THF and methanol were removed in vacuum, the resulting solution was filtered, and neutralized with 2 M hydrochloric acid. The precipitate was filtered off and dried in vacuum at room temperature. Corresponding amounts of the chemicals added and reaction times are provided for each hydrolysis product.

Tetrabutyl 9,9'-(pyrene-2,7-diyl)bis(9*H*-carbazole-3,6-dicarboxylate) (2)

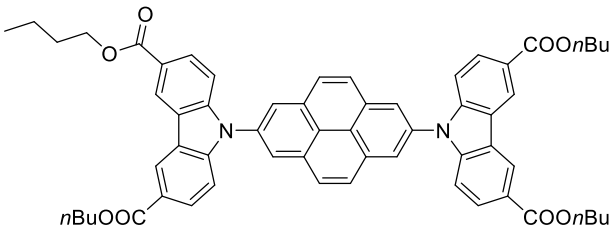

Synthesis conditions: 3.76 g (10.2 mmol) *n*-butyl ester **1**, 1.23 g (3.41 mmol) 2,7-dibromopyrene, 1.84 g (13.3 mmol) potassium carbonate, 323 mg (1.7 mmol) copper(I) iodide, 0.1 ml (0.91 mmol) *N,N'*-dimethylethylenediamine, 60 ml anhydr. 1,4 dioxane, 100 °C for 11 d; Flash column chromatography chloroform : *iso*-hexane : ethyl acetate – 1 : 0.33 : 0.03 (R_f 0.41); Yield: 0.7 g (20%) white powder.

^{1}H NMR (500 MHz, CHLOROFORM-*d*) δ (ppm): 1.05 (t, *J*=7.41 Hz, 3 H) 1.49 - 1.64 (m, 2 H) 1.78 - 1.92 (m, 2 H) 4.44 (t, *J*=6.62 Hz, 2 H) 7.53 (d, *J*=8.51 Hz, 1 H) 8.22 (dd, *J*=8.51, 1.58 Hz, 1 H) 8.29 (s, 1 H) 8.47 (s, 1 H) 9.03 (d, *J*=0.95 Hz, 1 H).

^{13}C NMR (126 MHz, CHLOROFORM-*d*) δ (ppm): 14.11 (s, 1 CH_3) 19.64 (s, 1 CH_2) 31.19 (s, 1 CH_2) 65.17 (s, 1 CH_2) 109.90 (s, 1 CH) 123.41 (s, 1 C) 123.57 (s, 1 C) 123.72 (s, 1 CH) 123.97 (s, 1 CH) 124.05 (s, 1 C) 128.63 (s, 1 CH) 128.66 (s, 1 C) 133.04 (s, 1 C) 134.93 (s, 1 C) 144.91 (s, 1 C) 167.32 (s, 1 C).

MALDI-TOF-MS (m/z): Calculated for $C_{60}H_{56}N_2O_8$: 859; found 859 $[M\text{-}C_4H_9OH]^+$.

Elemental analysis: Calculated: C: 77.23%; H: 6.05%; N: 3%; found: C: 77.27%; H: 6.144%; N: 2.88%.

9,9'-(Pyrene-2,7-diyl)bis(9H-carbazole-3,6-dicarboxylic acid), $H_4(L^{147})$

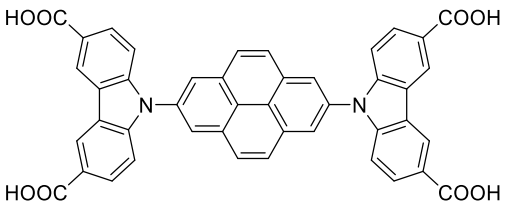

Synthesis conditions: 1.6 g (1.71 mmol) Ester **2**, 2.5 g (43.9 mmol) potassium hydroxide, 300 ml THF, 1 ml methanol, 2 ml H_2O + 1 ml H_2O after 1 d, 85 °C for 5 d; Yield: 650 g (91%) white powder.

^{1}H NMR (500 MHz, CHLOROFORM-*d*) δ (ppm): 7.63 (d, *J*=8.51 Hz, 1 H) 8.15 (dd, *J*=8.83, 1.58 Hz, 1 H) 8.48 (s, 1 H) 8.77 (s, 1 H) 9.08 (d, *J*=1.26 Hz, 1 H).

^{13}C NMR (126 MHz, DMSO-d_6) δ (ppm): 110.06 (s, 1 CH) 122.67 (s, 1 C) 122.94 (s, 1 C) 123.18 (s, 1 CH) 123.66 (s, 1 C) 123.75 (s, 1 CH) 128.39 (s, 1 CH) 128.46 (s, 1 CH) 132.41 (s, 1 C) 134.09 (s, 1 C) 144.03 (s, 1 C) 167.67 (s, 1 C).

MALDI-TOF-MS (m/z): Calculated for $C_{44}H_{24}N_2O_8$: 707; found 707 $[M\text{-}H]^+$.

Elemental analysis: Calculated ($C_{44}H_{23}N_2O_8$ 2.95·H_2O): C: 69.46%; H: 3.83%; N: 3.68%; found: C: 69.50%; H: 3.907%; N: 3.63%.

DRIFT, KBr, 298 K (cm^{-1}): 3074 (w, br), 2628 (w), 1905 (w), 1694 (s), 1630 (m), 1604 (s), 1479 (s), 1454 (m), 1409 (m), 1345 (m), 1288 (s), 1236 (s), 1159 (m), 1138 (w), 1028 (w), 1001 (w), 905 (w), 880 (w), 826 (m), 765 (s), 734 (w), 710 (m), 666 (w).

2,7-Dibromo-9,10-dihydrophenanthrene (3)

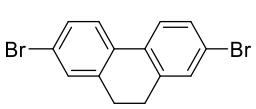

In a 250 ml flask 2 g (11.1 mmol) 9,10-hydrophenanthrene and 0.09 g (0.5 mmol) iron(III) chloride are suspended in 150 ml water. Over 30 min a solution of 1.26 ml (49.2 mmol) bromine in 50 ml water is added in dark conditions and stirred for 16 h at room temperature. The precipitate is filtered off, washed thoroughly with water, 30 ml 1 M aqueous sodium hydroxide solution, and again water. The yellow solid is recrystallized from 20 ml ethyl acetate to yield 2.7 g (71%) white powder.

R_f: 0.52 in *iso*-hexane.

^{1}H NMR (500 MHz, CHLOROFORM-*d*) δ (ppm): 2.84 (s, 2 H) 7.39 (d, *J*=1.89 Hz, 1 H) 7.43 (dd, *J*=8.28, 1.89 Hz, 1 H) 7.56 (d, *J*=8.28 Hz, 1 H).

^{13}C NMR (151 MHz, CHLOROFORM-*d*) δ (ppm): 28.53 (s, 1 CH_2) 76.79 (s, 1 CH) 77.00 (s, 1 C) 77.21 (s, 1 C) 121.50 (s, 1 C) 125.17 (s, 1 CH) 130.14 (s, 1 CH) 131.09 (s, 1 CH) 132.59 (s, 1 C) 139.09 (s, 1 C).

MALDI-TOF-MS (m/z): Calculated for $C_{14}H_{10}Br_2$: 337; found: 337 $[M]^+$.

Elemental analysis: Calculated: C: 49.74%; H: 2.98%; found: C: 48.63%; H: 3.021%.

Tetrabutyl 9,9'-(9,10-dihydrophenanthrene-2,7-diyl)bis(9*H*-carbazole-3,6-dicarboxylate) (4)

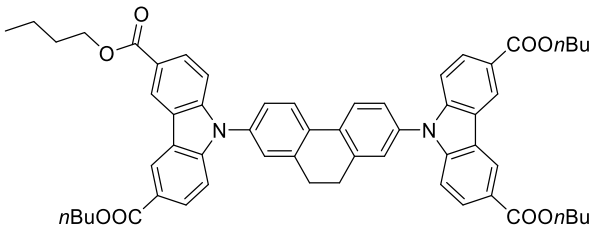

Synthesis conditions: 4.89 g (13.3 mmol) *n*-butyl ester **1**, 1.5 g (4.4 mmol) 2,7-dibromo-9,10-dihydrophenanthrene (**3**), 2.36 g (17.1 mmol) potassium carbonate, 400 mg (2.1 mmol) copper(I) iodine, 0.1 ml (0.91 mmol) *N,N'*-dimethylethylenediamine, 80 ml anhydr. 1,4 dioxane, 95 °C for 9 d; Flash column chromatography chloroform : *iso*-hexane : ethyl acetate – 1 : 0.33 : 0.03 (R_f 0.49); Yield: 1.8 g (45%) white powder.

^{1}H NMR (500 MHz, CHLOROFORM-*d*) δ (ppm): 1.05 (t, *J*=7.41 Hz, 6 H) 1.49 - 1.67 (m, 4 H) 1.77 - 1.93 (m, 4 H) 3.09 - 3.15 (m, 2 H) 4.43 (t, *J*=6.78 Hz, 4 H) 7.49 - 7.51 (m, 1 H) 7.51 - 7.54 (m, 2 H) 7.58 (dd, *J*=8.20, 2.21 Hz, 1 H) 8.11 (d, *J*=8.20 Hz, 1 H) 8.21 (dd, *J*=8.67, 1.73 Hz, 2 H) 8.96 (d, *J*=1.26 Hz, 2 H).

^{13}C NMR (126 MHz, CHLOROFORM-*d*) δ (ppm): 13.60 (s, 1 CH_3) 19.13 (s, 1 CH_2) 28.59 (s, 1 CH_2) 30.67 (s, 1 CH_2) 64.62 (s, 1 CH_2) 109.61 (s, 1 CH) 122.77 (s, 1 C) 122.93 (s, 1 CH) 125.37 (s, 1 CH) 125.48 (s, 1 CH) 126.36 (s, 1 CH) 127.95 (s, 1 CH) 133.52 (s, 1 C) 135.69 (s, 1 C) 139.24 (s, 1 C) 143.85 (s, 1 C) 166.83 (s, 1 C).

MALDI-TOF-MS (m/z): Calculated for $C_{58}H_{58}N_2O_8$: 837.3540; found: 837.2457 $[M\text{-}C_4H_9OH]^+$.

Elemental analysis: Calculated: C: 76.46%; H: 6.42%; N: 3.07%; found: C: 76.45%; H: 6.083%; N: 2.78%.

9,9'-(9,10-Dihydrophenanthrene-2,7-diyl)bis(9*H*-carbazole-3,6-dicarboxylic acid) ($H_4(L^{148})$)

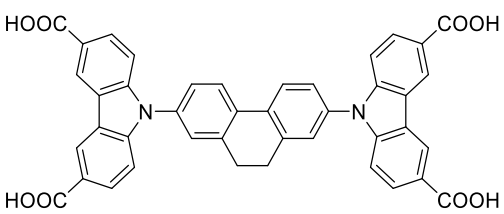

Synthesis conditions: 950 mg (1.04 mmol) Ester **4**, 2 g (35.1 mmol) potassium hydroxide, 80 ml THF, 1 ml methanol, 5 ml H_2O after 1 d, 85 °C for 48 h; Yield: 650 g (91%) white powder.

^{1}H NMR (500 MHz, DMSO-d_6) δ (ppm): 3.08 (s, 2 H) 7.57 (d, J=8.51 Hz, 2 H) 7.68 (dd, J=8.04, 2.05 Hz, 1 H) 7.71

(d, J=1.89 Hz, 1 H) 8.13 (dd, J=8.30, 1.80 Hz, 2 H) 8.28 (d, J=8.51 Hz, 1 H) 9.00 (d, J=1.58 Hz, 2 H) 12.81 (br. s., 2 H).

^{13}C NMR (126 MHz, DMSO-d_6) δ (ppm): 27.97 (s, 1 CH_2) 110.16 (s, 1 CH) 122.58 (s, 1 C) 123.08 (s, 1 CH) 123.46 (s, 1 C) 125.55 (s, 1 CH) 125.94 (s, 1 CH) 126.50 (s, 1 CH) 128.33 (s, 1 CH) 133.29 (s, 1 C) 135.26 (s, 1 C) 139.57 (s, 1 C) 143.44 (s, 1 C) 167.66 (s, 1 C).

Elemental analysis: Calculated ($C_{42}H_{26}N_2O_8$ 2.75·H_2O): C: 68.52%; H: 4.31%; N: 3.81%; found: C: 68.56%; H: 4.302%; N: 3.7%.

DRIFT, KBr, 298 K (cm^{-1}): 3073 (w, br), 2639 (w), 1902 (w), 1693 (s), 1630 (m), 1600 (s), 1491 (s)1362 (m), 1292 (s), 1235 (m), 1138 (m), 1027 (w)1008 (w), 905 (m), 825 (m), 769 (s), 734 (m), 696 (w), 640 (m), 597 (w), 573 (w).

Tetrabutyl 9,9'-(Ethyne-1,2-diylbis(4,1-phenylene))bis(9*H*-carbazole-3,6-dicarboxylate) (5)

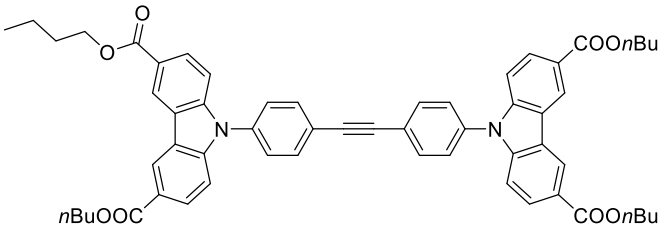

Synthesis conditions: 9.83 g (26.8 mmol) *n*-butyl ester **1**, 3 g (8.93 mmol) bis(4-bromophenyl)acetylene, 4.93 g (35.7 mmol) potassium carbonate, 847 mg (4.46 mmol) copper(I) iodine, 0.1 ml (0.91 mmol) *N,N'*-dimethylethylenediamine, 90 ml anhydr. 1,4 dioxane, 108 °C for 7 d; Flash column chromatography DCM : *iso*-hexane : ethyl acetate – 1 : 0.3 : 0.017 (R_f 0.51); Yield: 5.3 g (65%) white powder.

^{1}H NMR (500 MHz, CHLOROFORM-*d*) δ (ppm): 1.05 (t, *J*=7.41 Hz, 3 H) 1.53 - 1.61 (m, 2 H) 1.82 - 1.89 (m, 2 H) 4.43 (t, *J*=6.62 Hz, 2 H) 7.46 (d, *J*=8.83 Hz, 1 H) 7.62 (d, *J*=8.51 Hz, 1 H) 7.88 (d, *J*=8.20 Hz, 1 H) 8.20 (dd, *J*=8.83, 1.58 Hz, 1 H) 8.94 (d, *J*=1.26 Hz, 1 H).

^{13}C NMR (126 MHz, CHLOROFORM-*d*) δ (ppm): 14.10 (s, 1 CH_3) 19.62 (s, 1 CH_2) 31.17 (s, 1 CH_2) 65.16 (s, 1 CH_2) 109.93 (s, 1 CH) 123.30 (s, 1 CH) 123.56 (s, 1 CH) 123.69 (s, 1 C) 127.27 (s, 1 C) 128.55 (s, 1 CH) 129.72 (s, 1 CH) 133.74 (s, 1 CH) 134.46 (s, 1 C) 136.81 (s, 1 C) 144.08 (s, 1 C) 167.25 (s, 1 C).

MALDI-TOF-MS (m/z): Calculated for $C_{58}H_{56}N_2O_8$: 835; found 835 $[M\text{-}C_2H_5OH]^+$.

Elemental analysis: Calculated: C: 76.63%; H: 6.21%; N: 3.08%; found: C: 75.8%; H: 6.093%; N: 3.01%.

9,9'-(Ethyne-1,2-diylbis(4,1-phenylene))bis(9*H*-carbazole-3,6-dicarboxylic acid) ($H_4(L^{160})$)

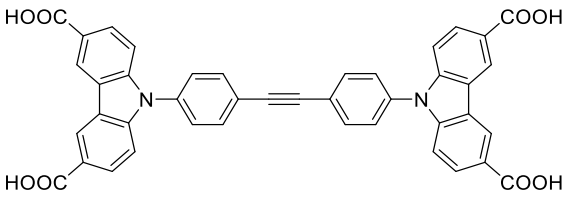

Synthesis conditions: 1 g (1.1 mmol) Ester **5**, 5 g (87.8 mmol) potassium hydroxide, 80 ml THF, 1 ml methanol, 5 ml H_2O, 90 °C for 16 h; Yield: 740 mg (98%) white powder.

^{1}H NMR (500 MHz, DMSO-d_6) δ (ppm): 7.53 (d, *J*=8.83 Hz, 1 H) 7.80 (d, *J*=8.51 Hz, 1 H) 7.96 (d, *J*=8.51 Hz, 1 H) 8.12 (dd, *J*=8.51, 1.58 Hz, 1 H) 9.00 (d, *J*=1.58 Hz, 1 H) 12.88 (br. s., 1 H).

^{13}C NMR (126 MHz, DMSO-d_6) δ (ppm): 90.07 (s, 1 C) 110.35 (s, 1 CH) 122.38 (s, 1 C) 123.05 (s, 1 C) 123.42 (s, 1 CH) 124.00 (s, 1 C) 127.70 (s, 1 CH) 128.72 (s, 1 CH) 133.84 (s, 1 CH) 136.52 (s, 1 C) 143.53 (s, 1 C) 167.94 (s, 1 C).

MALDI-TOF-MS (m/z): Calculated for $C_{42}H_{24}N_2O_8$: 684; found 684 $[M]^+$.

Elemental analysis: Calculated ($C_{42}H_{24}N_2O_8$ 2.6·H_2O): C: 68.96%; H: 4.02%; N: 3.83%; found: C: 68.86%; H: 3.915%; N: 3.75%.

DRIFT, KBr, 298 K (cm^{-1}): 3065 (w, br), 2642 (w), 1905 (w), 1693 (s), 1630 (m), 1600 (s), 1519 (s)1476 (m), 1412 (m), 1365 (m), 1286 (s), 1236 (s), 1184 (m), 1170 (m), 1137 (w)1108 (w), 1027 (w), 948 (w), 905 (w), 825 (m), 769 (s), 739 (w), 724 (w), 697 (w).

Tetrabutyl 9,9'-(ethane-1,2-diylbis(4,1-phenylene))bis(9*H*-carbazole-3,6-dicarboxylate) (6)

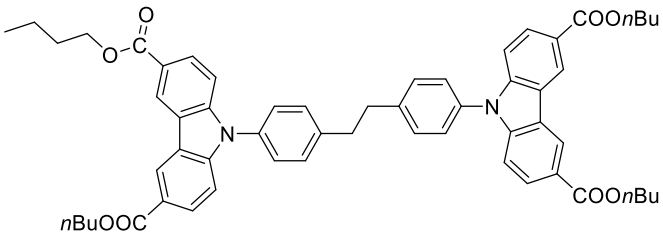

A 50 ml Schlenk flask was charged with 600 mg (0.66 mmol) acetylene **5** and100 mg 10% Pd on carbon and flushed with hydrogen. 30 ml anhydr. THF was added, hydrogen was bubbled through the suspension for 10 min. and stirred with 1.05 bar hydrogen pressure at room temperature for 48 h. The THF was removed in vacuum, the residual powder dissolved in chloroform and the suspension filtered over silica. The chloroform was removed in vacuum to yield 580 mg (97%) white powder.

R_f: 0.53 in DCM : *iso*-hexane : ethyl acetate – 1 : 0.3 : 0.017.

^{1}H NMR (500 MHz, BENZENE-d_6) δ (ppm): 1.04 (t, *J*=7.41 Hz, 3 H) 1.53 - 1.60 (m, 2 H) 1.81 - 1.89 (m, 2 H) 3.21 (s, 1 H) 4.42 (t, *J*=6.62 Hz, 2 H) 7.40 (d, *J*=8.83 Hz, 1 H) 7.53 (d, *J*=3.78 Hz, 1 H) 8.16 (dd, *J*=8.67, 1.73 Hz, 1 H) 8.94 (d, *J*=1.26 Hz, 1 H).

^{13}C NMR (126 MHz, BENZENE-d_6) δ (ppm): 13.83 (s, 1 CH_3) 19.36 (s, 1 CH_2) 30.92 (s, 1 CH_2) 37.49 (s, 1 CH_2) 64.83 (s, 1 CH_2) 77.56 (s, 1 CH_2) 109.71 (s, 1 CH) 122.99 (s, 1 CH) 123.04 (s, 1 C) 127.13 (s, 1 CH) 128.12 (s, 1 CH) 130.17 (s, 1 CH) 134.49 (s, 1 C) 141.85 (s, 1 C) 144.26 (s, 1 C) 167.10 (s, 1 C).

MALDI-TOF-MS (m/z): Calculated for $C_{58}H_{60}N_2O_8$: 839; found 839 $[M\text{-}C_2H_5OH]^+$.

Elemental analysis: Calculated: C: 76.29%; H: 6.62%; N: 3.07%; found: C: 76.2%; H: 5.931%; N: 2.8%.

9,9'-(Ethane-1,2-diylbis(4,1-phenylene))bis(9*H*-carbazole-3,6-dicarboxylic acid) ($H_4(L^{162})$)

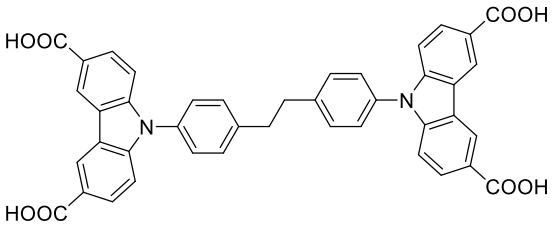

Synthesis conditions: 520 g (0.57 mmol) Ester **6**, 1 g (17.6 mmol) potassium hydroxide, 60 ml THF, 2 ml methanol, 2 ml H_2O, 80 °C for 16 h; Yield: 350 mg (89%) white powder.

^{1}H NMR (600 MHz, DMSO-d_6) δ (ppm): 3.20 (s, 1 H) 7.45 (d, *J*=8.66 Hz, 1 H) 7.63 - 7.67 (m, 1 H) 7.67 - 7.73 (m, 1 H) 8.11 (dd, *J*=8.66, 1.88 Hz, 1 H) 9.00 (d, *J*=1.51 Hz, 1 H) 12.51 - 13.15 (m, 1 H).

^{13}C NMR (151 MHz, DMSO-d_6) δ (ppm): 36.63 (s, 1 CH_2) 109.86 (s, 1 CH) 122.39 (s, 1 C) 123.00 (s, 1 CH) 123.26 (s, 1 C) 126.89 (s, 1 CH) 128.26 (s, 1 CH) 130.36 (s, 1 CH) 133.64 (s, 1 C) 142.17 (s, 1 C) 143.61 (s, 1 C) 167.62 (s, 1 C).

MALDI-TOF-MS (m/z): Calculated for $C_{42}H_{28}N_2O_8$: 688; found: 688 $[M]^+$.

Elemental analysis: Calculated ($C_{42}H_{28}N_2O_8$ 2.5·H_2O): C: 68.87%; H: 3.99%; N: 3.82%; found: C: 68.39%; H: 2.35%; N: 3.71%.

DRIFT, KBr, 298 K (cm^{-1}): 3065 (w, br), 2641 (w), 1689 (s), 1630 (m), 1598 (s), 1516 (s), 1477 (m), 1415 (s)1352 (m), 1273 (s), 1171 (m), 1134 (m), 1026 (w), 904 (m), 821 (m), 768 (s), 725 (m), 693 (w),

665 (w), 640 (m), 600 (w).

Tetrabutyl 9,9'-(ethene-1,2-diylbis(4,1-phenylene))(E)-bis(9*H*-carbazole-3,6-dicarboxylate) (7)

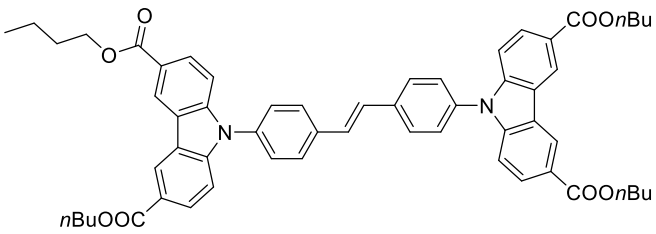

Synthesis conditions: 6.56 g (17.8 mmol) *n*-butylester **1**, 1.93 g (5.95 mmol) 4,4'-dibromo-trans-stilbene, 3.2 g (23.7 mmol) potassium carbonate, 475 mg (2.49 mmol) copper(I) iodide, 0.1 ml (0.91 mmol) *N,N'*-dimethylethylenediamine, 60 ml anhydr. 1,4 dioxane, 108 °C for 10 d; Flash column chromatography chloroform: *iso*-hexane : ethyl acetate – 1 : 0.17 : 0.003 (R_f 0.49)

Yield: 3.8 g (70%) white powder

^{1}H NMR (500 MHz, CHLOROFORM-*d*) δ (ppm): 1.05 (t, *J*=7.41 Hz, 6 H) 1.50 - 1.66 (m, 4 H) 1.79 - 1.91 (m, 4 H) 4.43 (t, *J*=6.62 Hz, 4 H) 7.36 (s, 1 H) 7.46 (d, *J*=8.83 Hz, 2 H) 7.61 (d, *J*=8.51 Hz, 2 H) 7.85 (d, *J*=8.51 Hz, 2 H) 8.19 (d, *J*=8.51 Hz, 2 H) 8.95 (d, *J*=1.26 Hz, 2 H).

^{13}C NMR (126 MHz, CHLOROFORM-*d*) δ (ppm): 13.83 (s, 1 CH_3) 19.36 (s, 1 CH_2) 30.93 (s, 1 CH_2) 64.87 (s, 1 CH_2) 109.77 (s, 1 CH) 123.02 (s, 1 CH) 123.20 (s, 1 C) 123.24 (s, 1 C) 127.32 (s, 1 CH) 128.21 (s, 1 CH) 128.24 (s, 1 CH) 128.83 (s, 1 CH) 135.91 (s, 1 C) 137.12 (s, 1 C) 144.06 (s, 1 C) 167.06 (s, 1 C).

HRMS-MALDI (m/z): Calculated for $C_{58}H_{58}N_2O_8$: 837.3540; found 837.42787 $[M\text{-}C_2H_5OH]^+$

Elemental analysis: Calculated: C: 76.46%; H: 6.42%; N: 3.07%; found: C: 76.33%; H: 6.14%; N: 2.82%.

(E)-9,9'-(Ethene-1,2-diylbis(4,1-phenylene))bis(9*H*-carbazole-3,6-dicarboxylic acid) ($H_4(L^{161})$)

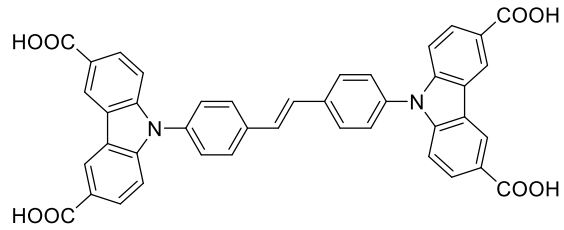

Synthesis conditions: 2.7 g (2.63 mmol) Ester **7**, 2.3 g (40.4 mmol) potassium hydroxide, 200 ml THF, 2 ml methanol, 10 ml H_2O, 85 °C for 48 h.

Yield: 2 g (99%) yellow powder

^{1}H NMR (500 MHz, DMSO-d_6) δ (ppm): 6.66 (d, *J*=8.51 Hz, 2 H) 6.76 (s, 1 H) 6.88 (d, *J*=8.51 Hz, 2 H) 7.16 (d, *J*=8.51 Hz, 2 H) 7.26 (dd, *J*=8.51, 1.58 Hz, 2 H) 8.14 (d, *J*=1.26 Hz, 2 H) 11.96 (br. s., 2 H)

^{13}C NMR (126 MHz, DMSO-d_6) δ (ppm): 110.03 (s, 1 CH) 122.55 (s, 1 C) 123.04 (s, 1 CH) 123.44 (s, 1 C) 127.26 (s, 1 CH) 128.32 (s, 1 CH) 128.44 (s, 1 CH) 128.78 (s, 1 CH) 135.07 (s, 1 C) 137.18 (s, 1 C) 143.42 (s, 1 C) 167.46 (s, 1 C) 167.63 (s, 1 C)

Elemental analysis: Calculated: C: 73.46%; H: 3.82%; N: 4.08%; found: C: 68.43%; H: 3.78%; N: 4.05%;

DRIFT, KBr, 298 K (cm^{-1}): 3064 (w, br), 2643 (w), 1905 (w), 1689 (s), 1630 (m), 1600 (s), 1518 (s), 1476 (m), 1412 (m), 1365 (m), 1286 (s), 1236 (s), 1182 (m), 1170 (m), 1137 (w)1108 (w), 1028 (m), 948 (w), 905 (w), 826 (m), 771 (s), 739 (w), 728 (w), 693 (w).

Tetrabutyl 9,9'-(1,4-phenylenebis(methylene))bis(9*H*-carbazole-3,6-dicarboxylate) (8)

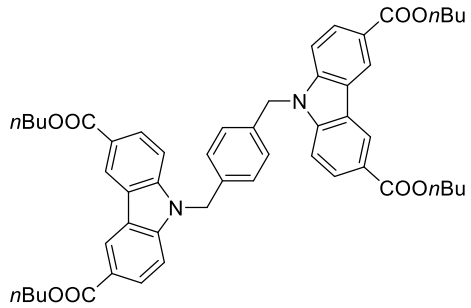

Synthesis conditions: 8.34 g (22.7 mmol) *n*-butyl ester **1**, 2 g (7.58 mmol) dibromo-p-xylene, 4.93 g (35.7 mmol) potassium carbonate, 686 mg (3.62 mmol) copper(I) iodide, 0.1 ml (0.91 mmol) *N,N'*-dimethylethylenediamine, 150 ml anhydr. 1,4 dioxane, 95 °C for 5 d; Flash column chromatography DCM : *iso*-hexane : ethyl acetate – 1 : 0.4 : 0.01 (R_f 0.6); Yield: 1.2 g (19%) white powder.

^{1}H NMR (500 MHz, CHLOROFORM-*d*) δ (ppm): 1.02 (t, *J*=7.41 Hz, 2 H) 1.54 (dq, *J*=14.94, 7.42 Hz, 2 H) 1.82 (quin, *J*=7.17 Hz, 2 H) 4.39 (t, *J*=6.62 Hz, 2 H) 5.51 (s, 1 H) 7.01 (s, 1 H) 7.34 (d, *J*=8.51 Hz, 1 H) 8.16 (dd, *J*=8.51, 1.26 Hz, 1 H) 8.88 (d, *J*=1.26 Hz, 1 H).

^{13}C NMR (126 MHz, CHLOROFORM-*d*) δ (ppm): 13.56 (s, 1 CH_3) 19.09 (s, 1 CH_2) 30.66 (s, 1 CH_2) 46.22 (s, 1 CH_2) 64.54 (s, 1 CH_2) 108.52 (s, 1 CH) 122.44 (s, 1 C) 122.65 (s, 1 C) 122.80 (s, 1 C) 126.69 (s, 1 CH) 127.89 (s, 1 CH) 135.48 (s, 1 C) 143.44 (s, 1 C) 166.83 (s, 1 C).

MALDI-TOF-MS (m/z): Calculated for $C_{52}H_{56}N_2O_8$: 763; found: 763 $[M\text{-}C_4H_9OH]^+$.

Elemental analysis: Calculated: C: 74.62%; H: 6.74%; N: 3.35%; found: C: 74.3%; H: 6.725%; N: 3.28%.

9,9'-(1,4-Phenylenebis(methylene))bis(9*H*-carbazole-3,6-dicarboxylic acid) ($H_4(L^{159})$)

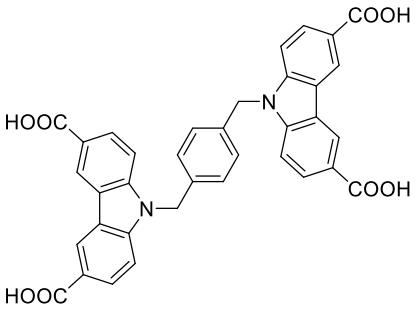

Synthesis conditions: 900 g (1.08 mmol) Ester **8**, 2.6 g (45.7 mmol) potassium hydroxide, 100 ml THF, 1 ml methanol, 2 ml H_2O, 90 °C for 24 h; Yield: 480 mg (73%) white powder.

^{1}H NMR (500 MHz, DMSO-d_6) δ (ppm): 5.68 (s, 1 H) 7.08 (s, 1 H) 7.70 (d, *J*=8.51 Hz, 1 H) 8.04 (dd, *J*=8.51, 1.58 Hz, 1 H) 8.87 (d, *J*=1.58 Hz, 1 H) 12.67 (br. s., 1 H).

^{13}C NMR (126 MHz, DMSO-d_6) δ (ppm): 45.62 (s, 1 CH_2) 109.79 (s, 1 CH) 122.09 (s, 1 C) 122.55 (s, 1 C) 122.81 (s, 1 CH) 127.06 (s, 1 CH) 127.80 (s, 1 CH) 136.30 (s, 1 C) 143.34 (s, 1 C) 167.70 (s, 1 C).

Elemental analysis: Calculated ($C_{36}H_{24}N_2O_8$ 7.3·H_2O): C: 58.11%; H: 5.23%; N: 3.76%; found: C: 57.44%; H: 4.56%; N: 3.74%.

DRIFT, KBr, 298 K (cm^{-1}): 3062 (w, br), 2643 (w), 1682 (s), 1630 (m), 1598 (s), 1515 (w), 1482 (m), 1416 (m), 1385 (m), 1308 (s), 1203 (s), 1147 (m), 1119 (m), 1052 (w), 1026 (w), 904 (w), 855 (w), 819 (m), 769 (s), 722 (m), 642 (w), 597 (w).

3 Synthesis of Metal-Organic Frameworks

Synthesis of MOF Single Crystals

For the synthesis of crystals large enough to allow for SCXRD higher amounts of DMF (*N,N* Dimethylformamide) as well as acetic acid as modulator were used. The reactions were generally carried out according to the following procedure. The reaction conditions are listed in. The solvothermal reactions were carried out in a 10 ml Pyrex® tube. The organic ligand was dissolved in indicated amounts of DMF and acetic acid by sonication at room temperature. Indicated amounts of $Cu(NO_3)_2 \cdot 3H_2O$ were added and dissolved by sonication. The sealed tube was placed in an oven at 80 °C for the indicated timeframe. Synthesis conditions are summarized in Supplementary Table 1.

Supplementary Table 1. Reaction conditions for the synthesis of MOF single crystals (> 100 µm). No yield was determined and all reactions were carried out at 80 °C.

Material ID	m_{Ligand} (mg)	n_{Ligand} (µmol)	$m_{Cu(NO3)2\cdot3H2O}$ (mg)	$n_{Cu(NO3)2\cdot3H2O}$ (µmol)	$V_{Acetic\ acid}$ (µl)	$n_{Acetic\ acid}$ (mmol)	*Eq.per ligand*	V_{DMF} (ml)	$t_{Reaction}$ (d)	Morphology
DUT-49	10	15.1	9.5	39.3	0.5	8.7	577	4	5	Cubic
DUT-147	5	7.1	8.5	35.2	0.2	3.5	495	10	6	Cubic
DUT-148	10	14.6	8.8	36.4	0.08	1.4	96	3	3	Cubic
DUT-159	5	8.2	4.8	19.9	0.2	3.5	428	3	4	hex. Plates
DUT-160	10	14.6	8.8	36.4	0.33	5.8	395	4	2	Cuboct.
DUT-161	10	14.6	8.8	36.4	0.33	5.8	395	4	2	Cuboct.
DUT-162	10	14.5	8.8	36.4	0.8	14.0	963	5	5	Cuboct.

Synthesis of MOF powders

Synthesis of large-scale MOF powders was conducted in DMF (with the exception of DUT-162 where L^{162} was found to be insoluble in higher concentrations; *N*-Methyl-2-pyrrolidone (NMP) was used in the synthesis of DUT-162). The reaction was carried out in a round bottom flask, and the reaction mixture was stirred and heated at 80 °C using an oil bath. All reactions were conducted in the following manner: The linker was dissolved in the indicated amount of solvent; corresponding amounts of modulator were added and the solution was stirred at 80 °C. To this solution indicated amounts of $Cu(NO_3)_2 \cdot 3H_2O$ were added and dissolved, the flask was closed and the reaction mixture stirred for the indicated time at 80 °C. Afterwards the MOF powders were separated from the mother liquid via centrifugation and washed with fresh DMF for at least three times over three days. The powder was kept solvated with DMF at all times. The reaction conditions are summarized in Supplementary Table 2.

Supplementary Table 2. Reaction conditions for the synthesis of DUT-49 and analogous MOF powders synthesis at 80 °C .

Material ID	m_{ligand} (mg)	n_{ligand} (mmol)	$m_{Cu(NO3)2\cdot3H2O}$ (mg)	$n_{Cu(NO3)2\cdot3H2O}$ (mmol)	$V_{Acetic\ acid}$ (ml)	$n_{Acetic\ acid}$ (mmol)	V_{DMF} (ml)	$t_{Reaction}$ (h)	Yield (%)[a]	Mean crystal size/ SD (nm)
DUT-49	150	0.23	140	0.58	7.5	131.1	60	144	39	14861±5069
DUT-147	250	0.35	215	0.89	6	104.9	230	96	68	8385 ±5279
DUT-148	100	0.15	87.9	0.36	2	35.0	30	48	81	7872 ±4500
DUT-159	250	0.41	202	0.84	0.5	8.7	40	48	40	n. a.
DUT-160	1000	1.46	880	3.64	10	174.8	200	48	47	4475 ± 1969
DUT-161	500	0.74	441	1.82	4	70.1	95	48	48	6241 ± 3103
DUT-162	120	0.17	100	0.41	0.3	5.2	20*	48	71	4517 ± 3223

[a] yield based on n_{Ligand} after activation, actual yields of reaction may be higher. *NMP was used instead of DMF

4 Supercritical Activation of MOF Powders

All MOF samples analyzed in this work were activated using this protocol which is based on previous reports[1, 6]: Activation in this context refers to the removal of the solvent or guest molecules from the pores of the MOF. After synthesis the MOF powders were suspended in fresh solvent used for the synthesis (DMF or NMP) and the solvent was exchanged at least 9 times over a period of at least two days. Afterwards the solvent was replaced by anhydr. ethanol (for DUT-49) or anhydr. acetone (for DUT-49(17) and all other MOF materials) in multiple washing cycles (at least 6 times over three days). The material was then dried (solvent removal) using a previously well described protocol involving supercritical CO_2.[217] The ethanol/acetone suspended MOF powder was placed in glass filter frits in a Jumbo Critical Point Dryer 13200J AB (SPI Supplies) which was subsequently filled with liquid CO_2 (99.995% purity) at 288 K and 5 MPa. To ensure a complete substitution of the solvent by CO_2, the liquid in the autoclave was exchanged with fresh CO_2 at least 18 times over a period of 5 days using a valve at the bottom of the autoclave. The temperature and pressure were then risen beyond the supercritical point of CO_2 to 308 K and 10 MPa and kept until the temperature and pressure was constant. The supercritical CO_2 was steadily released over 3 h and the dry powder was transferred and stored in an argon filled glove box. To ensure complete removal of the solvent (especially from the open metal sites of the Cu-paddle-wheels) additional activation at 120 - 423 K in a Schlenk-tube under dynamic vacuum of 10^{-4} kPa for at least 24 h was performed.

5 Elemental Analysis of MOF samples

For elemental analysis the desolvated powders were placed in Sn-sample holders under inert atmosphere in a glove box and sealed to avoid contamination with humidity. The given results are the mean values obtained from three individual measurements. Results are summarized in Supplementary Table 3.

Supplementary Table 3. CHNS elemental analysis of activated MOF powders.

	Calculated (%)				***Experimental (%)***			
Material ID	**C**	**H**	**N**	**S**	**C**	**H**	**N**	**S**
DUT-49	61.3	2.57	3.57	0	59.85	2.542	3.64	0
DUT-147	63.54	2.42	3.37	0	60.78	2.397	3.5	0
DUT-148	62.3	2.74	3.46	0	61.49	2.539	3.75	0
DUT-159	58.78	2.74	3.81	0	62.66	3.677	4.88	0
DUT-160	62.45	2.5	3.47	0	61.04	2.752	5.05	0
DUT-161	62.03	2.81	3.11		60.66	3.165	4.09	0
DUT-162	62.14	2.98	3.45	0	61.29	3.382	3.71	0

6 Thermogravimetric analysis of MOF samples

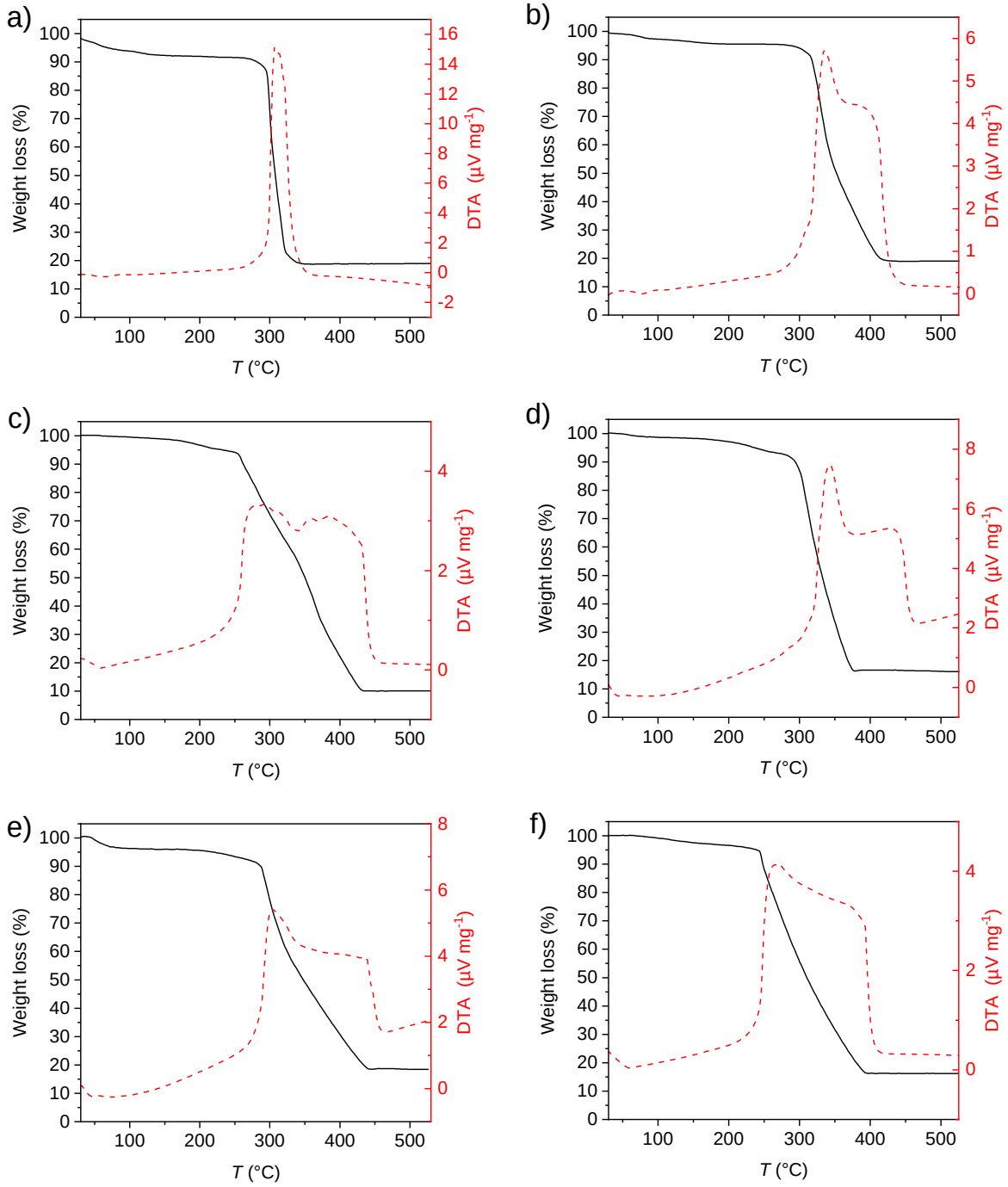

Supplementary Figure 2. Thermogravimetric analysis of a) DUT-147, b) DUT-148, c) DUT-159, d) DUT-160, e) DUT-161 and, f) DUT-162.

7 Powder X-ray diffraction (PXRD) of MOF samples

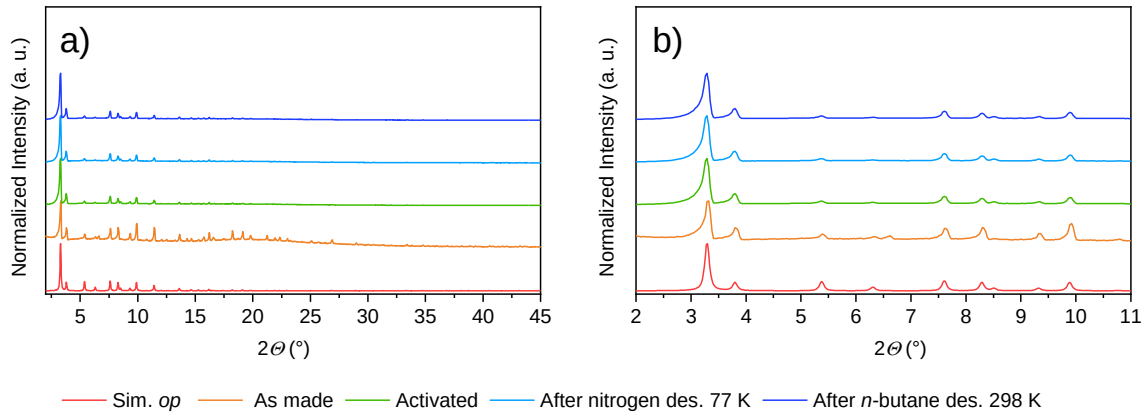

Supplementary Figure 3. PXRD patterns of DUT-147 under different conditions.

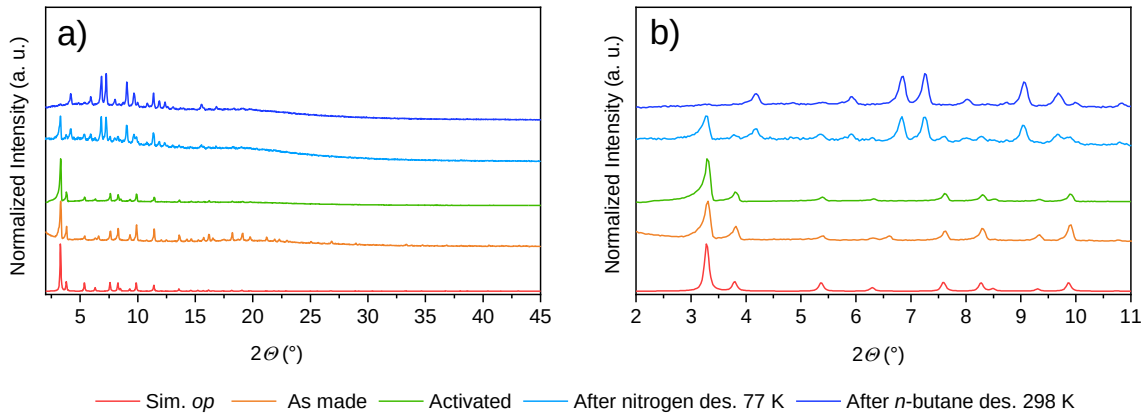

Supplementary Figure 4. PXRD patterns of DUT-148 under different conditions.

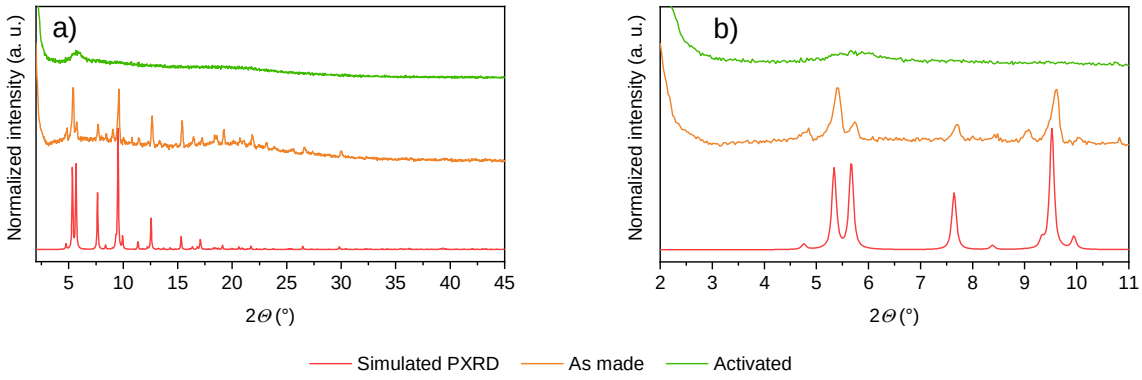

Supplementary Figure 5. PXRD patterns of DUT-159 under different conditions.

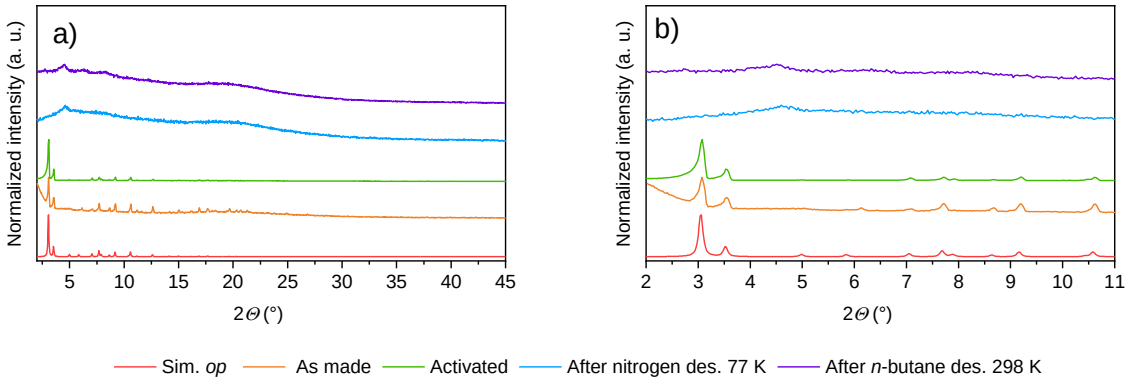

Supplementary Figure 6. PXRD patterns of DUT-160 under different conditions.

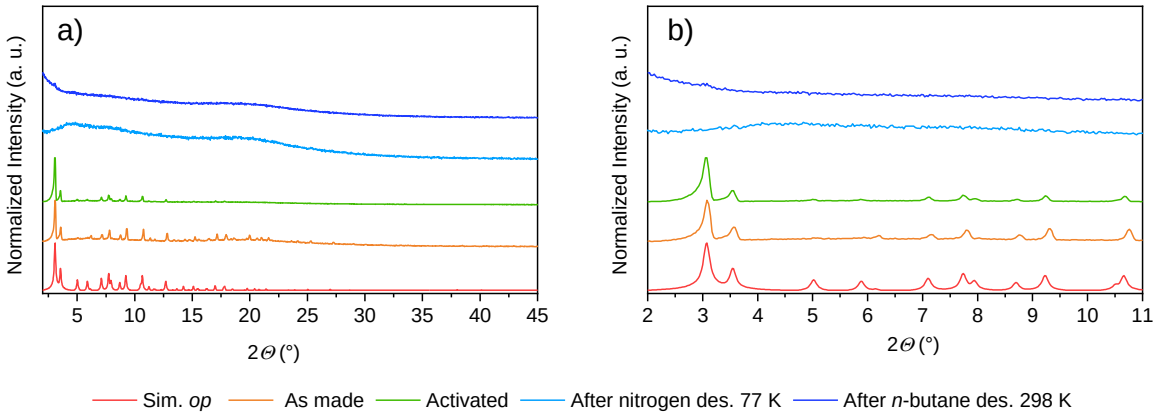

Supplementary Figure 7. PXRD patterns of DUT-161 under different conditions.

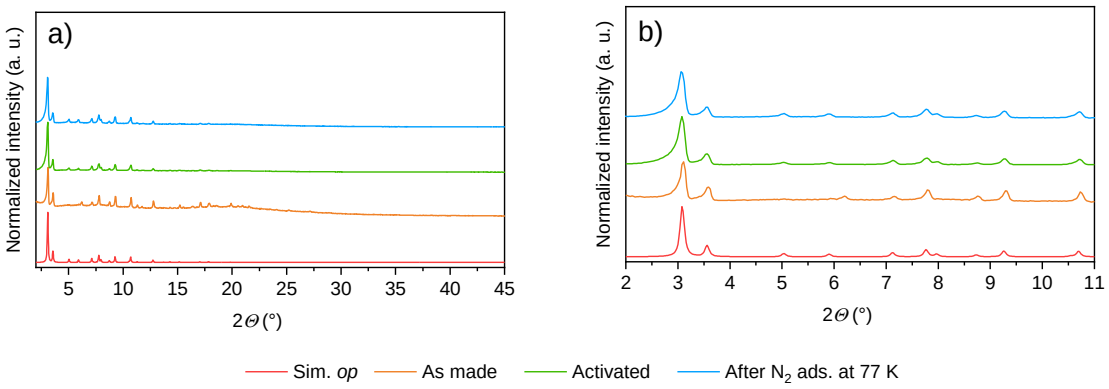

Supplementary Figure 8. PXRD patterns of DUT-162 under different conditions.

8 Scanning Electron microscopy and size distribution of MOF samples

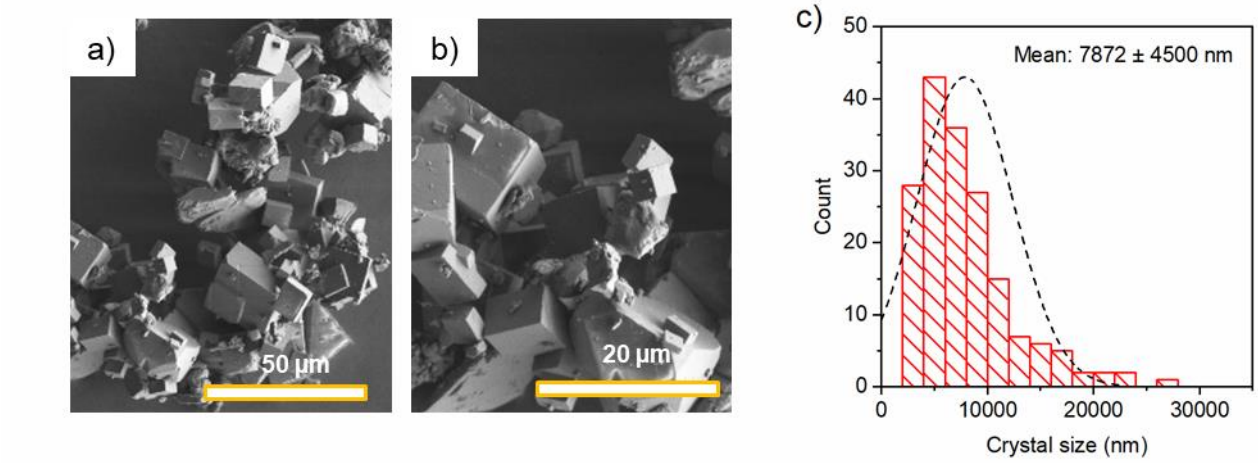

Supplementary Figure 9. Scanning electron microscopy images of a,b) DUT-147, c) Experimental crystal size distribution (red histogram) and distribution curve (black dashed line).

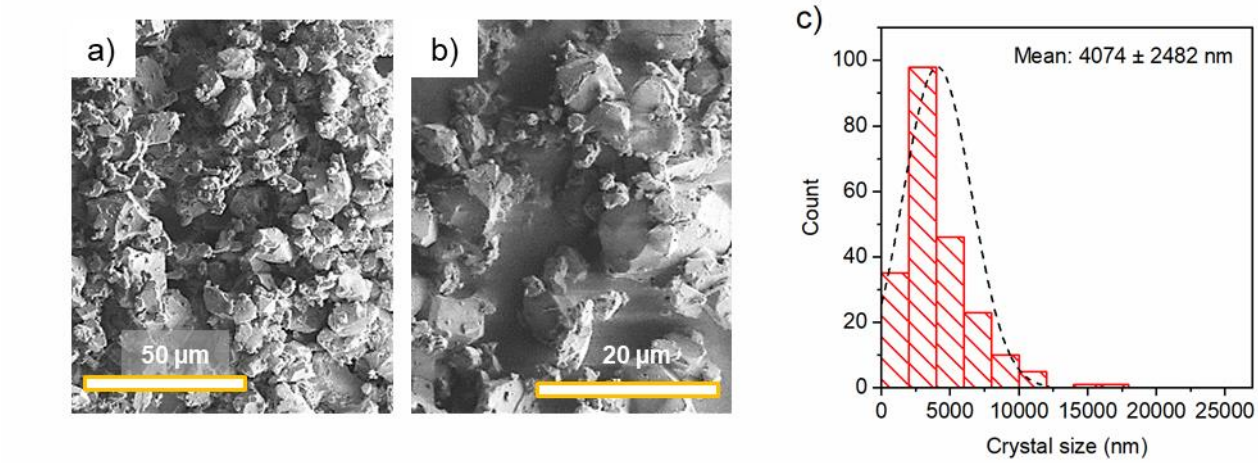

Supplementary Figure 10. Scanning electron microscopy images of a,b) DUT-148, c) Experimental crystal size distribution (red histogram) and distribution curve (black dashed line).

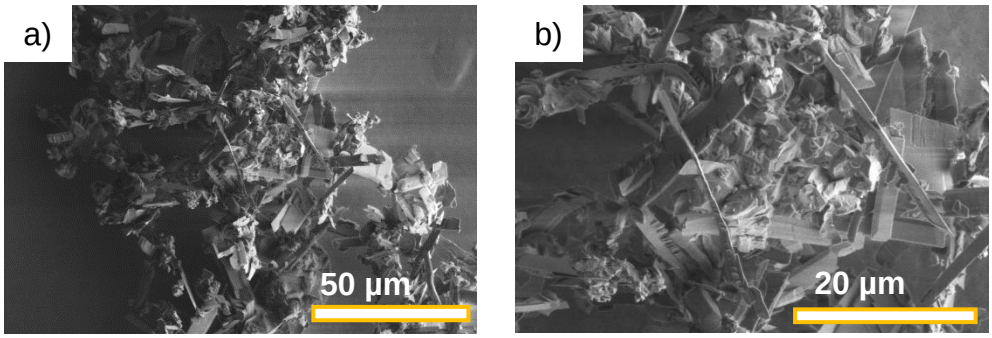

Supplementary Figure 11. Scanning electron microscopy images of activated DUT-159 at different magnifications.

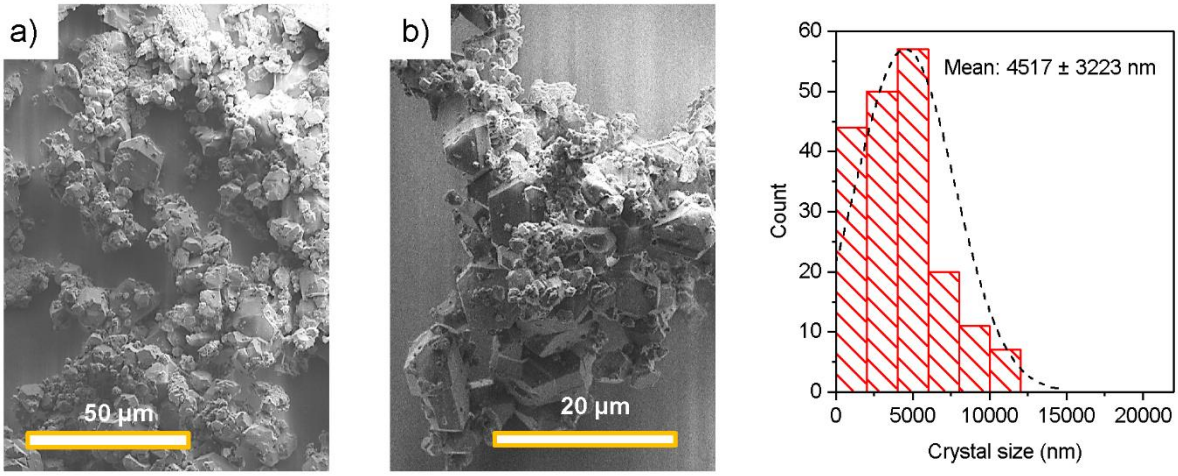

Supplementary Figure 12. Scanning electron microscopy images of a,b) DUT-160, c) Experimental crystal size distribution (red histogram) and distribution curve (black dashed line).

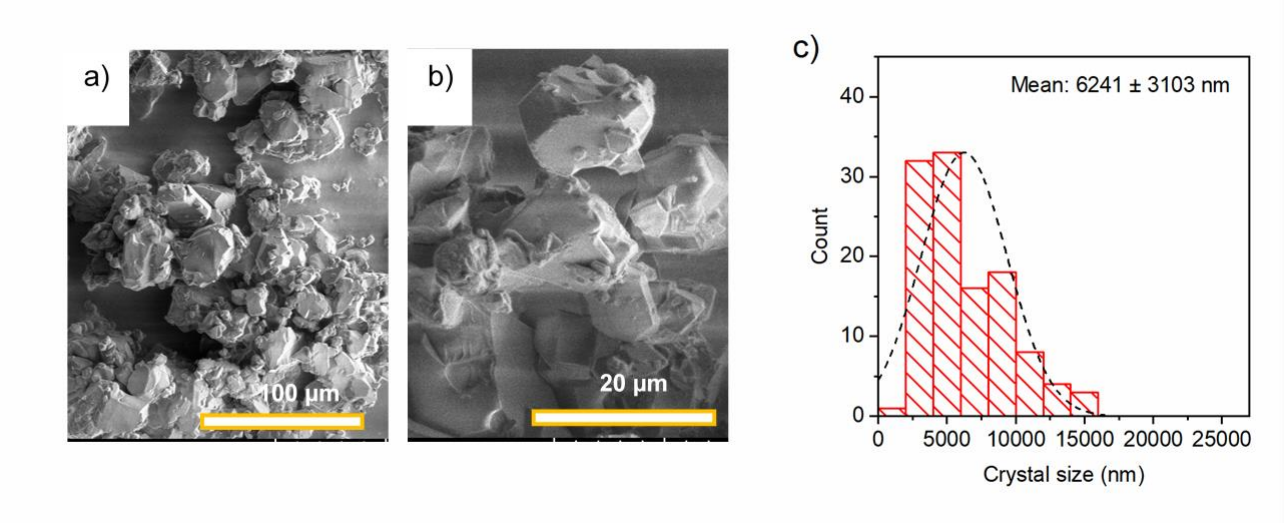

Supplementary Figure 13. Scanning electron microscopy images of a,b) DUT-161, c) Experimental crystal size distribution (red histogram) and distribution curve (black dashed line).

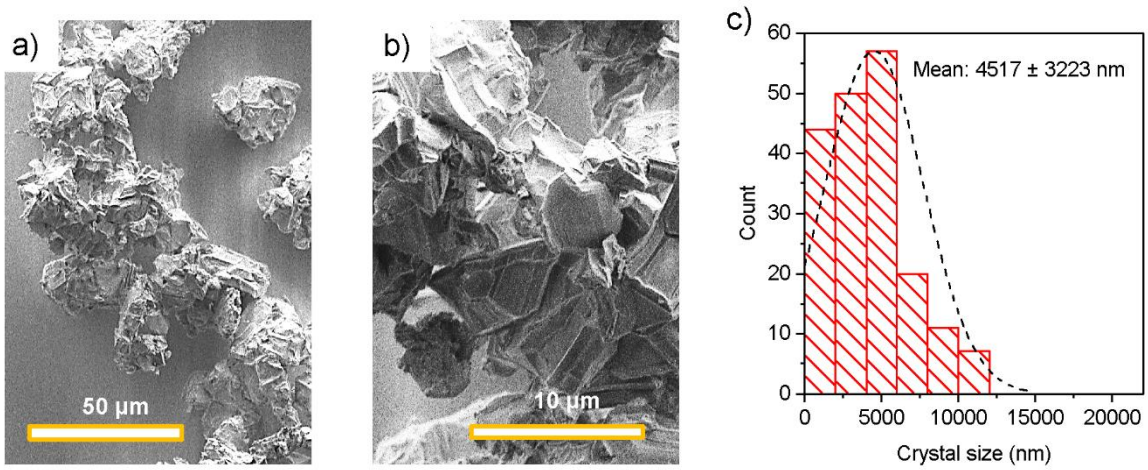

Supplementary Figure 14. Scanning electron microscopy images of a,b) DUT-162, c) Experimental crystal size distribution (red histogram) and distribution curve (black dashed line).

9 Gas Adsorption Experiments of MOF samples

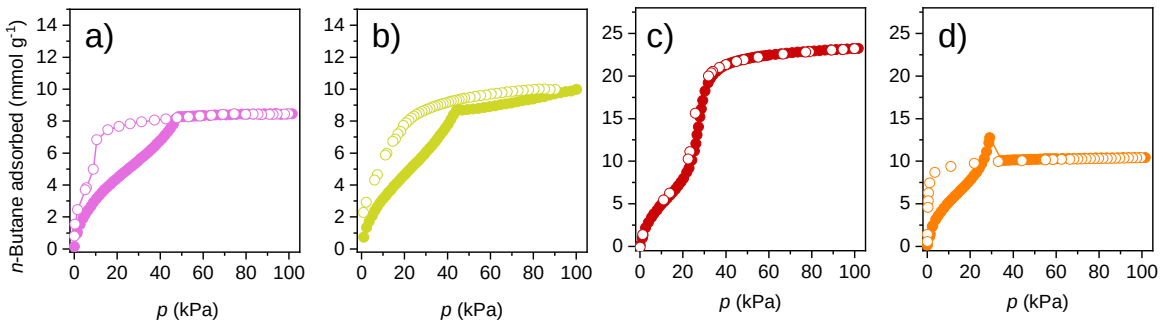

Supplementary Figure 15. *n*-Butane physisorption isotherms at 298 K of a) DUT-160, b) DUT-161, c) DUT-147, and d) DUT-148. Closed symbols adsorption, open symbols desorption.

Routine for sample recycling

The following routine is a literal adaption from our previous work.[7] In our previous studies on NGA the transition upon desorption was found to be irreversible.[8] Consequently, for each adsorption measurement a new sample of DUT-49 had to be used to record individual isotherms. To overcome this extensive usage of sample amount a routine was developed to repeatedly reproduce DUT-49 NGA transitions. This procedure was previously described in two references[1, 8] and was primarily applied in the characterization of methane and ethane for which experiments were first conducted at elevated temperatures and then stepwise decreased until structural transitions were observed and then after desorption the regeneration protocol applied.

In general, adsorbed molecules can be removed from the pores of DUT-49 if the guest molecules are in a supercritical state (reversible adsorption). This fact is used in the initial supercritical activation of DUT-49 using carbon dioxide. When analyzing the adsorption behavior upon adsorption of methane it becomes obvious that the isotherms become reversible at temperatures beyond the critical point (for methane around 150 K). Thus, methane can be removed from the pores of DUT-49*op* by increasing the temperature beyond this point while maintaining saturation pressure in the measuring cell. This method of regeneration has some experimental limitations: The increase in temperature while maintaining saturation pressure of the adsorptives can lead to high pressures. Thus, this method of regeneration can only be performed using high pressure equipment. For experiments conducted at pressures below 100 kPa in the BELSORP-max instrument, each experiment was performed on a fresh sample.

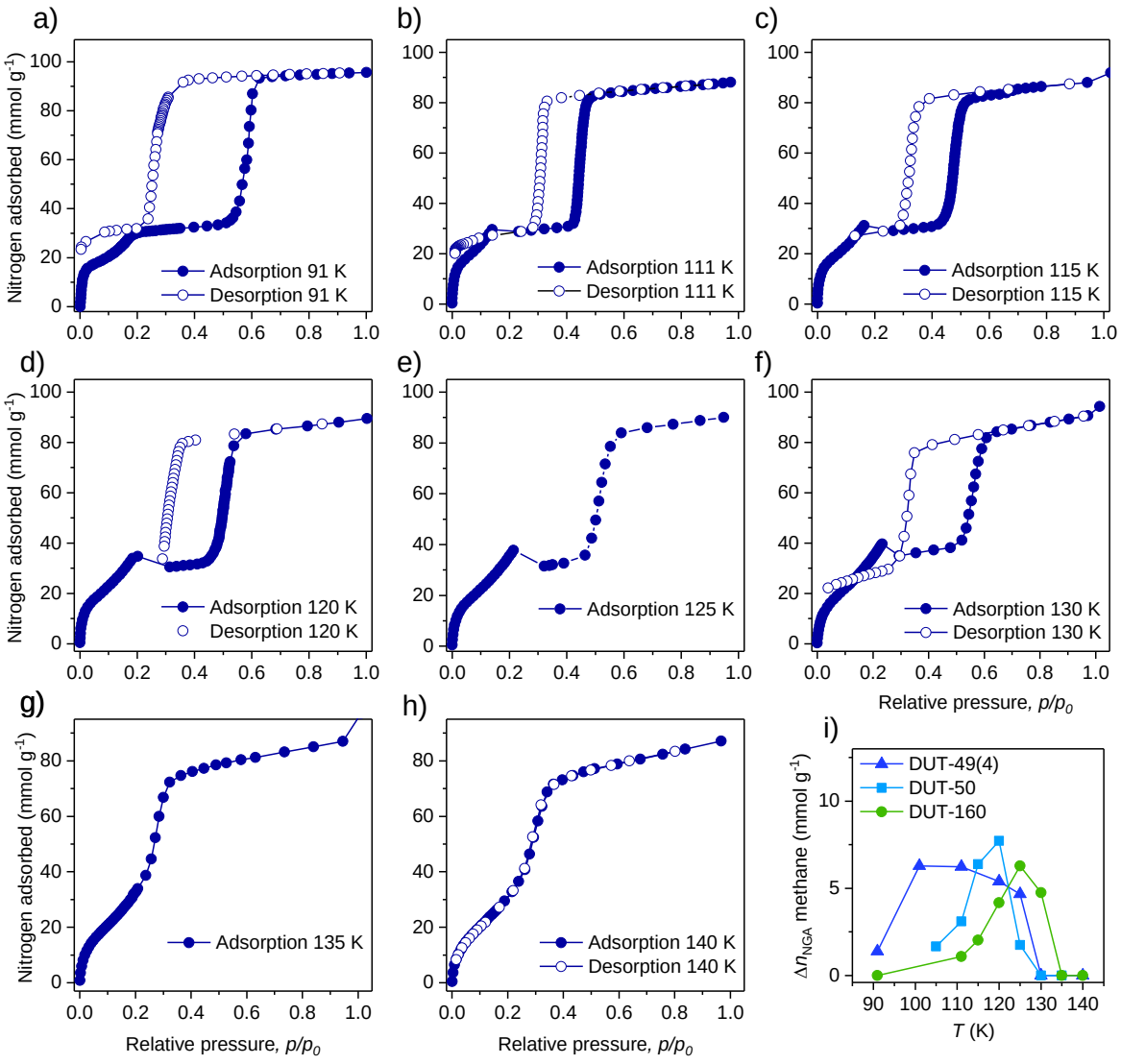

Supplementary Figure 16. Methane adsorption/desorption isotherms on DUT-160 at 91 K (a), 111 K (b), 115 K (c), 120 K (d), 125 K (e), 130 K (f), 135 K (g) and 140 K (h). Adsorption in closed symbols, desorption in open symbols. i) Evolution of Δn_{NGA} at different temperatures in comparison to DUT-49(4) and DUT-50.

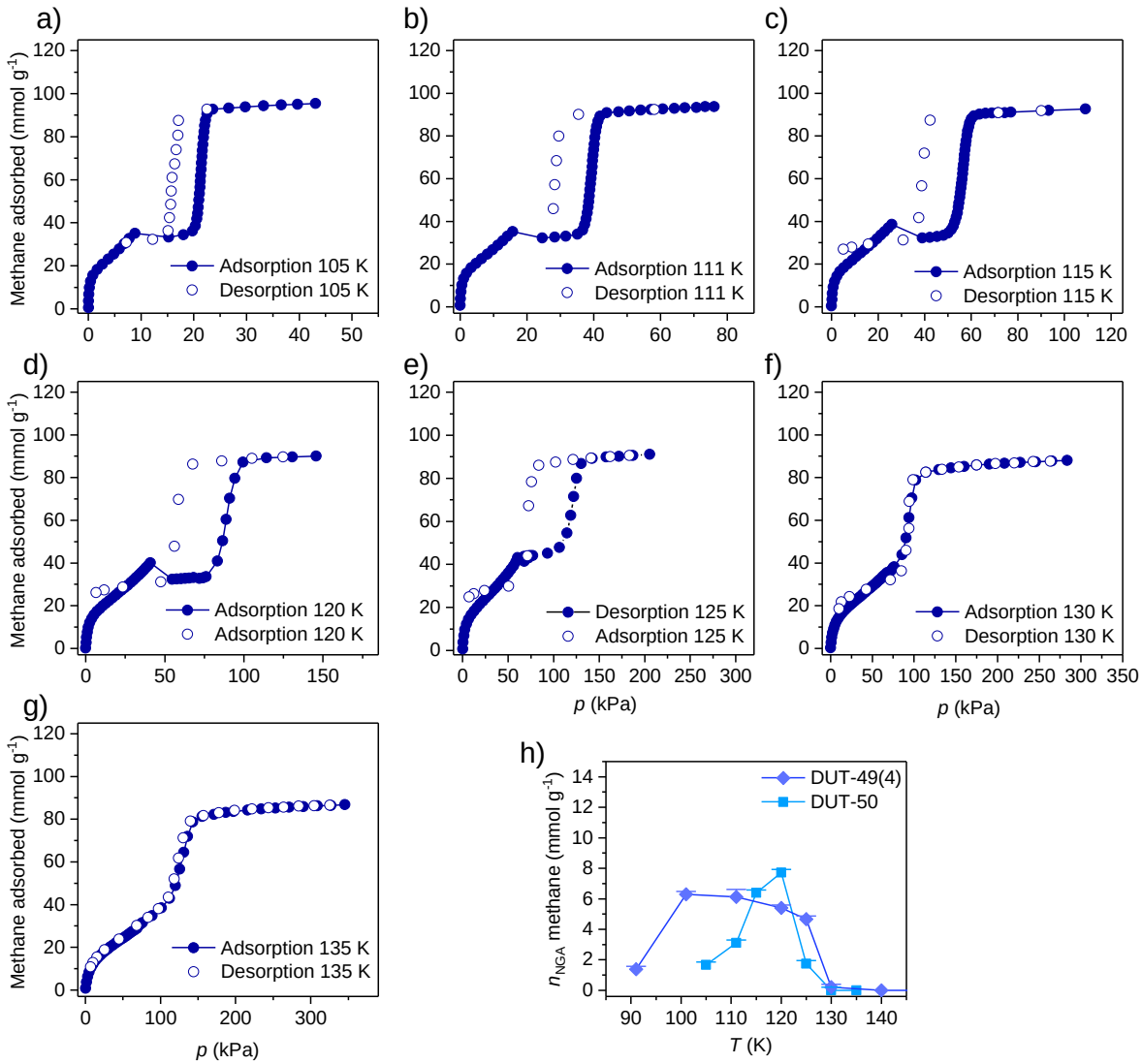

Supplementary Figure 17. Methane adsorption (closed symbols) /desorption (open symbols) isotherms on DUT-50 at a) 105 K, b) 111 K, c) 115 K, d) 120 K, e) 125 K, f) 130 K, and g) 135 K. h) Evolution of Δn_{NGA} at different temperatures in comparison to DUT-49(4).

10 Mercury (Hg) intrusion experiments

Mercury intrusion has been successfully used in the past to provoke the contraction of microporous metal organic frameworks[1, 9] MOF powders were preliminary outgassed under secondary vacuum at 110°C overnight. The so-obtained powders were loaded into a powder penetrometer of 3.1126 cm^3 volume with a stem volume of 0.4120 cm^3 using a glove box (Jacomex P-BOX) under argon atmosphere H_2O < 5 ppm. The mercury intrusion experiments were carried out using a Micromeritics AutoPore IV 9500 allowing a range of pressure applied from 0.003 to 413 MPa. Before the compression experiment, the powders were outgassed at ~6.5 Pa for 15 minutes. The collected volume of intruded mercury was corrected by a blank recorded in the same conditions of temperature and pressure using the same penetrometer to obtain the absolute contracted volume as a function of the pressure.

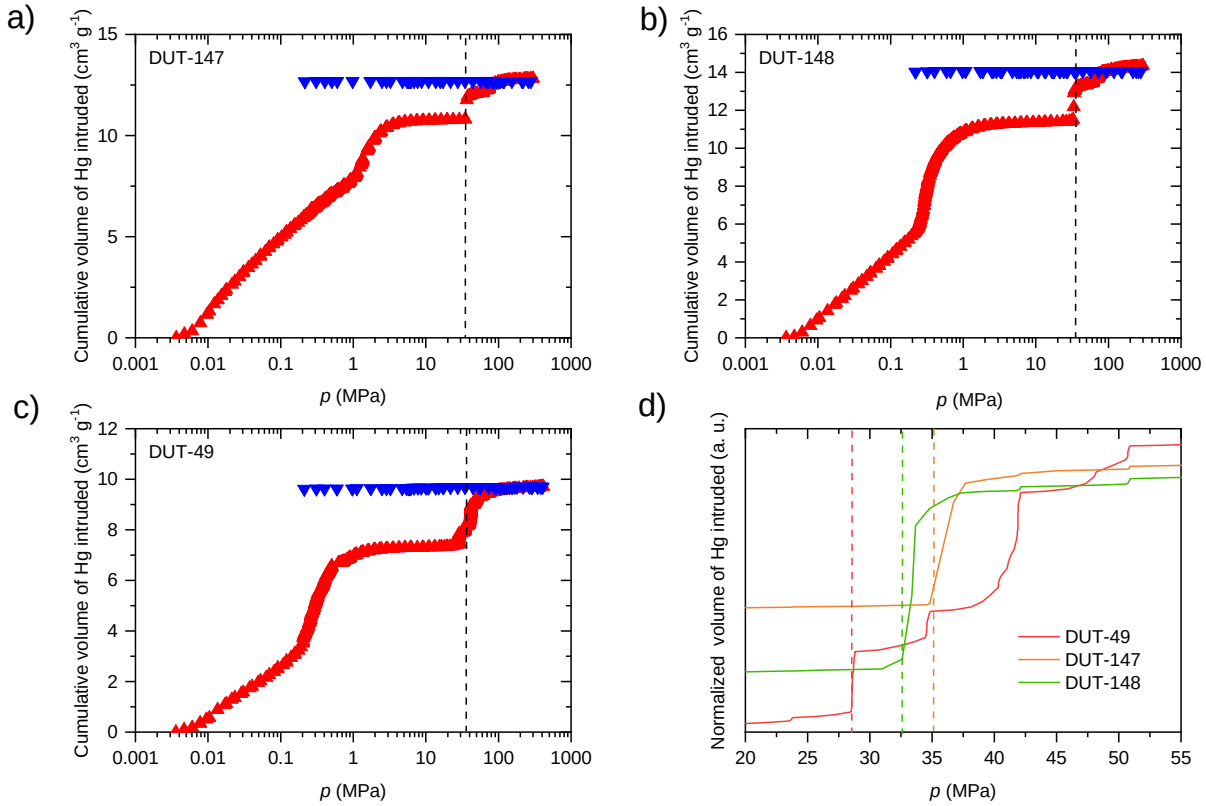

Supplementary Figure 18. Mercury intrusion curves (pressure increase red, pressure release blue) for a) DUT-147, b) DUT-148, c) DUT-49 (taken from reference[1]), and d) comparison of the three intrusion curves. Pressure for unit cell compression indicated as dashed line.

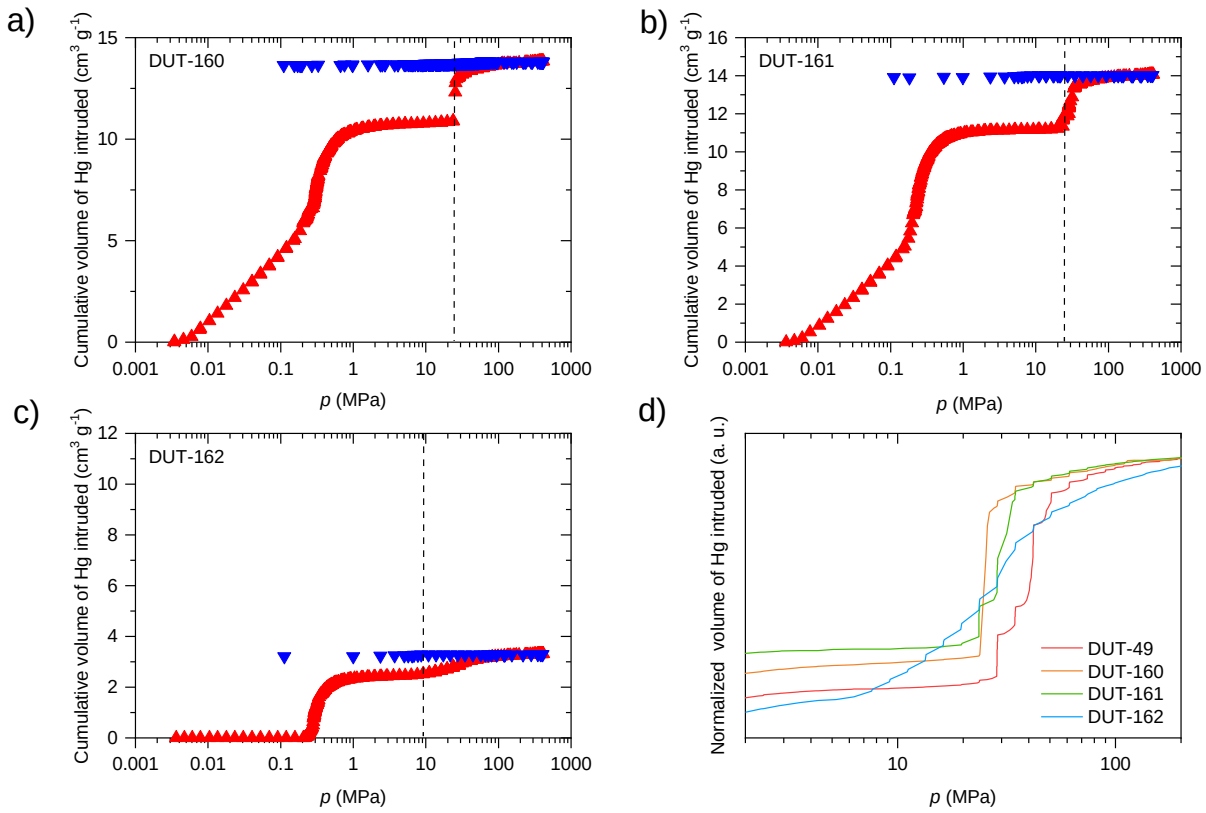

Supplementary Figure 19. Mercury intrusion curves (pressure increase red, pressure release blue) for a) DUT-160, b) DUT-161, c) DUT-162, and d) comparison of the three intrusion curves. Pressure for unit cell compression indicated as dashed line.

The bulk modulus *K* of the pristine phase for the studied solids can be estimated form the compression curves obtained by mercury intrusion using the following equation $K = V_0\left(\frac{dp}{dV}\right)$. Where V_0 is the volume of the initial phase. The bulk modulus is then related to the slope of the linear domain of the cumulative volume of intruded mercury as a function of the applied pressure (Supplementary Figure 19, Supplementary Figure 18) which is defined by $\alpha = \left(\frac{dV}{dp}\right)$. In mercury intrusion experiments *V* is expressed in volume of Hg intruded per gram of sample. Hence this volume correspond to $V_{Hg} = \frac{V_0 \times N_A}{Z \times M_{sample}}$.Table S1 contains the results of the linear fitting and bulk moduli estimation following the relation defined by Henke et al.[10]

$$K = \frac{V_0 \times N_A}{\alpha \times Z \times M_{sample}}$$

Supplementary Table 4. Unit cell volumes, formula per unit cell, molar mass, slope of the mercury intrusion curves and bulk moduli determined form both DUT-49, -147, -148, -160, -161 and -162 and 147.

	DUT-49	DUT-147	DUT-148	DUT-160	DUT-161	DUT-162
V_0 unit cell volume ($Å^3$)	100071	100221	100804	125827	123209	121950
Z, number of formula per unit cell	24	24	24	24	24	24
M, molar mass ($g.mol^{-1}$)	783.70	831.73	809.72	807.71	809.72	811.74
α, slope of the mercury intrusion curve ($mL.g^{-1}.MPa^{-1}$)	3.80×10^{-3}	2.19×10^{-3}	2.67×10^{-3}	6.92×10^{-3}	4.16×10^{-3}	6.79×10^{-3}
K, Bulk modulus (MPa)	843	1518	1170	543	883	534

11 Single crystal X-ray diffraction

Single crystals of DUT-147, DUT-148 and DUT-159, DUT-160, and DUT-161 with dimensions ranging from 30 µm to 80 µm were prepared in a borosilicate glass capillary (d = 0.3 mm) with small amount of DMF. The capillaries were sealed with wax from both sides in order to avoid contact with ambient atmosphere. The datasets were collected at BESSY MX BL14.2 and BL14.3 beamlines of Helmholtz-Zentrum Berlin für Materialien und Energie[11] at 298 K. After short test scans, the crystal symmetry and scan range were determined in each particular case using iMosflm program[12]. The φ-scans with oscillation step of 0.5° were used for data collection. All datasets were processed automatically using XDSAPP 2.0 software[13]. Crystal structures were solved by direct methods and refined by full matrix least-squares on F^2 using SHELX-2016/4 program package[14]. All non-hydrogen atoms were refined in anisotropic approximation. Hydrogen atoms were refined in geometrically calculated positions using "riding model" with $U_{iso}(H)$=1.2$U_{iso}(C)$. In the crystal structures of DUT-147 and DUT-160, the pyrene and phenyl rings are disordered over two positions. Dihydrophenanthrene, stilbene and dibenzyl backbones in DUT-148, DUT-161, and DUT-162 structures, respectively are disordered over four positions, which were refined with corresponding reduced occupancies. During the refinement of DUT-148, DUT-161, and DUT-162 distance restraints were used to fix the geometry of dihydrophenanthrene, stilbene and dibenzyl fragments. Disordered guest molecules could not be refined unambiguously from the difference Fourier map, hence, SQUEEZE routine in PLATON was used to generate the reflection intensities with subtracted solvent contribution[15].

CCDC-2003150-2003155 contain the supplementary crystallographic data for DUT-147, DUT-148, DUT-159, DUT-160 and DUT-161 correspondingly. These data can be obtained free of charge from the Cambridge Crystallographic Data Centre via www.ccdc.cam.ac.uk/data_request/cif.

Supplementary Table 5. Experimental data on single crystal X-ray diffraction for as made phases of DUT-147, DUT-148 and DUT-159.

	DUT-147	**DUT-148**	**DUT-159**
Empirical formula	$C_{44}H_{20}Cu_2N_2O_8 \cdot 2H_2O$	$C_{42}H_{22}Cu_2N_2O_8 \cdot 2H_2O$	$C_{36}H_{20}Cu_2N_2O_{10} \cdot 2H_2O$
Formula weight, g mol^{-1}	867.76	845.75	767.62
Crystal system, space group	cubic, $Fm\bar{3}m$	cubic, $Fm\bar{3}m$	trigonal, $R\bar{3}m$
Unit cell dimensions, Å	a = 46.450(5)	a = 46.540(5)	a = 23.110(3) c = 49.600(10)
Unit cell volume, Å^3	100221(35)	100804(35)	22941(8)
Z	24	24	9
Calculated density, g·cm^{-3}	0.343	0.333	0.500
Temperature, K	293	293	293
Wavelength, Å	0.88561	0.88561	0.89499
Absorption coefficient, mm^{-1}	0.5	0.497	0.814
F(000)	8928 (after SQUEEZE)	10224 (after SQUEEZE)	3492 (after SQUEEZE)
Θ range, °	0.956 – 33.070	0.954 – 36.062	1.382 - 33.930
Limiting indices	-45 ≤ h ≤ 52 -56 ≤ k ≤ 48 -55 ≤ l ≤ 17	-50 ≤ h ≤ 44 -58 ≤ k ≤ 48 -58 ≤ l ≤ 18	-28 ≤ h ≤ 28 -28 ≤ k ≤ 28 -61 ≤ l ≤ 51
Reflections collected / unique	46235 / 4582	53443 / 5638	48209 / 5577
R_{int}	0.0681	0.0486	0.0653
Data / parameters	4582 / 106	5638 / 106	5577 / 124
GooF on F^2	0.981	1.021	0.972
Final R indices [I>2$\sigma(I)$]	R_1 = 0.0626/ wR_2 = 0.1862	R_1 = 0.0676 / wR_2 = 0.2043	R_1 = 0.0579 / wR_2 = 0.2003
wR indices (all data)	R_1 = 0.1082/ wR_2 = 0.2344	R_1 = 0.1102 / wR_2 = 0.2490	R_1 = 0.0745 / wR_2 = 0.2252
Largest diff. peak / hole, eÅ^{-3}	0.465 / -0.522	1.102/ -0.417	0.357 / -0.274

Supplementary Table 6. Experimental data on single crystal X-ray diffraction for as made phases of DUT-160, DUT-161 and DUT-162.

	DUT-160	**DUT-161**	**DUT-162**
Empirical formula	$C_{42}H_{20}Cu_2N_2O_8 \cdot 2H_2O$	$C_{42}H_{22}Cu_2N_2O_8 \cdot 2H_2O$	$C_{42}H_{24}Cu_2N_2O_8 \cdot 2H_2O$
Formula weight, g mol^{-1}	843.74	841.69	847.77
Crystal system, space group	cubic, $Fm\bar{3}m$	cubic, $Fm\bar{3}m$	cubic, $Fm\bar{3}m$
Unit cell dimensions, Å	a = 50.110(6)	a = 49.760(6)	a = 49.590(6)
Unit cell volume, Å^3	125827(44)	123209(43)	121950(42)
Z	24	24	24
Calculated density, g·cm^{-3}	0.266	0.272	0.276
Temperature, K	293	293	293
Wavelength, Å	0.89499	0.89499	0.88561
Absorption coefficient, mm^{-1}	0.398	0.406	0.411
F(000)	10176 (after SQUEEZE)	10224 (after SQUEEZE)	10272 (after SQUEEZE)
Θ range, °	0.886 – 28.112	0.893 - 30.832	0.896 – 33.535
Limiting indices	-52 ≤ h ≤ 51 -52 ≤ k ≤ 50 -52 ≤ l ≤ 52	-24 ≤ h ≤ 56 -56 ≤ k ≤ 55 -56 ≤ l ≤ 27	-61 ≤ h ≤ 27 -59 ≤ k ≤ 61 -59 ≤ l ≤ 16
Reflections collected / unique	140813 / 3736	56402 / 4651	58786 / 5731
R_{int}	0.0578	0.0994	0.0648
Data / parameters	3736 / 101	4651 / 106	5731 / 106
GooF on F^2	1.083	1.021	0.917
Final R indices [I>2$\sigma(I)$]	R_1 = 0.0577 / wR_2 = 0.1921	R_1 = 0.0555 / wR_2 = 0.1714	R_1 = 0.0670 / wR_2 = 0.1932
wR indices (all data)	R_1 = 0.0755/ wR_2 = 0.2254	R_1 = 0.0869 / wR_2 = 0.2094	R_1 = 0.1467 / wR_2 = 0.2603
Largest diff. peak / hole, eÅ^{-3}	0.522 / -0.350	0.347 / -0.341	0.451 / -0.285

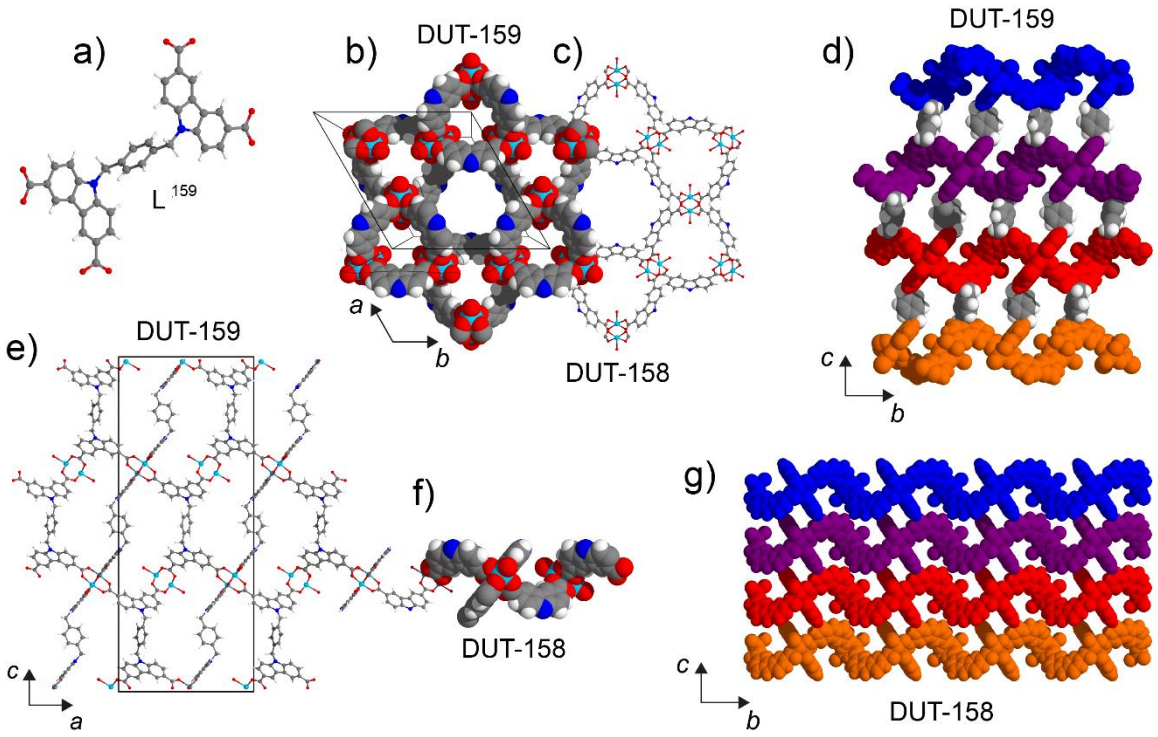

Supplementary Figure 20. a) L^{159} in the conformation present in DUT-159, b) Unit cell along *c*-direction of DUT-159 and c) DUT-158. d) DUT-159 along a-direction, individual Cu(cdc) layers are coloured in orange, red, purple and blue. e) Unit cell along *b*-direction of DUT-159 and f) DUT-158. g) DUT-158 along a-direction, individual Cu(cdc) layers are coloured in orange, red, purple and blue. Colour code: Hydrogen (white), carbon (grey), nitrogen (blue), oxygen (red), and copper (turquois).

12 In situ Powder X-ray Diffraction

In situ-PXRD studies and parallelised gas adsorption were measured at KMC-2 beamline of the BESSY II synchrotron[16], operated by Helmholtz-Zentrum Berlin für Materialien und Energie. Self-designed automated instrumentation, based on the volumetric adsorption instrument and closed-cycle Helium cryostat, equipped with adsorption chamber with beryllium domes was used in all experiments[17]. PXRD patterns were measured at constant wavelength λ = 0.15406 nm (E = 8048 eV) in transmission geometry. Because of the bulky cryostat, the sample holder cannot rotate during experiments, however an average crystallite size in the range of 2-15 µm and using an area 2D detector (Vantec 2000, Bruker) allowed to record diffraction images with reasonable particle statistics. Each 2D image was measured with 31 s exposure. For each experiment 10-12 mg of sample were used. In order cut off reflections coming from the crystalline Be-dome, tungsten slits with 5 mm aperture were mounted on the detector cone. The obtained diffraction images were integrated using DATASQUEEZE 2.2.9[18] with further processing in FITYK 0.9 software[19]. For all automated measurements the physisorption isotherms were measured using equilibrium settings for pressure change of 0.1% within 300 s. In case of the manual measurements, each pressure was set manually and PXRD patterns were measured after the pressure in the cell was stabilized for at least 300 s. PXRD patterns during adsorption and desorption of methane at 111 K on DUT-161 (Supplementary Figure 24) and nitrogen at 75.5 K on DUT-148 (Supplementary Figure 23) were measured in the automatic mode. PXRD patterns, measured during adsorption and desorption of *n*-butane at 273 K on DUT-147 (Supplementary Figure 21) and DUT-148 (Supplementary Figure 22) and DUT-160 (Supplementary Figure 25) and PXRD patterns with methane loading at 111 K on DUT-160 (Supplementary Figure 26) were measured in manual mode.

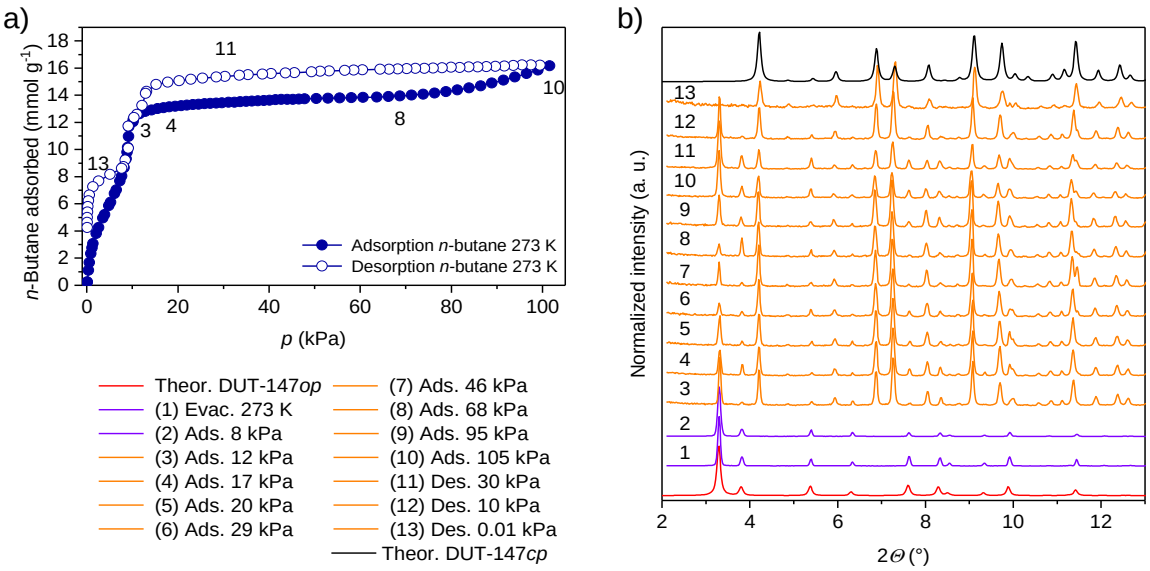

Supplementary Figure 21. *In situ* PXRD in parallel to *n*-butane physisorption at 273 K of DUT-147: a) Adsorption-desorption isotherm, selected points are labeled by numbers. Filled symbols correspond to adsorption, empty symbols to desorption. b) PXRD patterns, color code: DUT-147*cp* (orange), DUT-147*op* (purple), simulated pattern *op* (red) and *cp* (black).

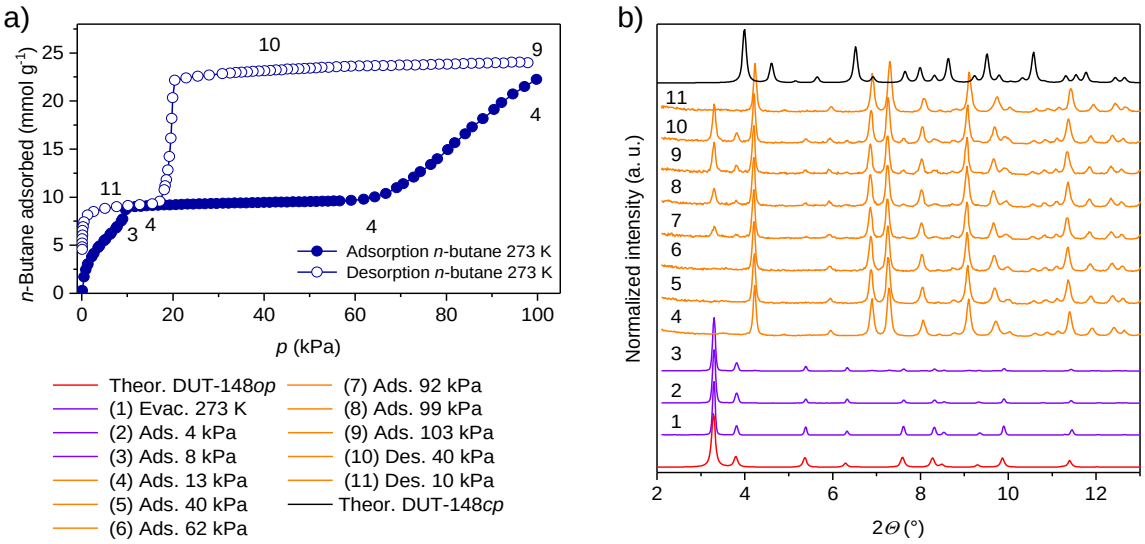

Supplementary Figure 22. *In situ* PXRD in parallel to *n*-butane physisorption at 273 K of DUT-148: a) Adsorption-desorption isotherm, selected points are labeled by numbers. Filled symbols correspond to adsorption, empty symbols to desorption. b) PXRD patterns, color code: DUT-148*cp* (orange), DUT-148*op* (purple), simulated pattern *op* (red) and *cp* (black).

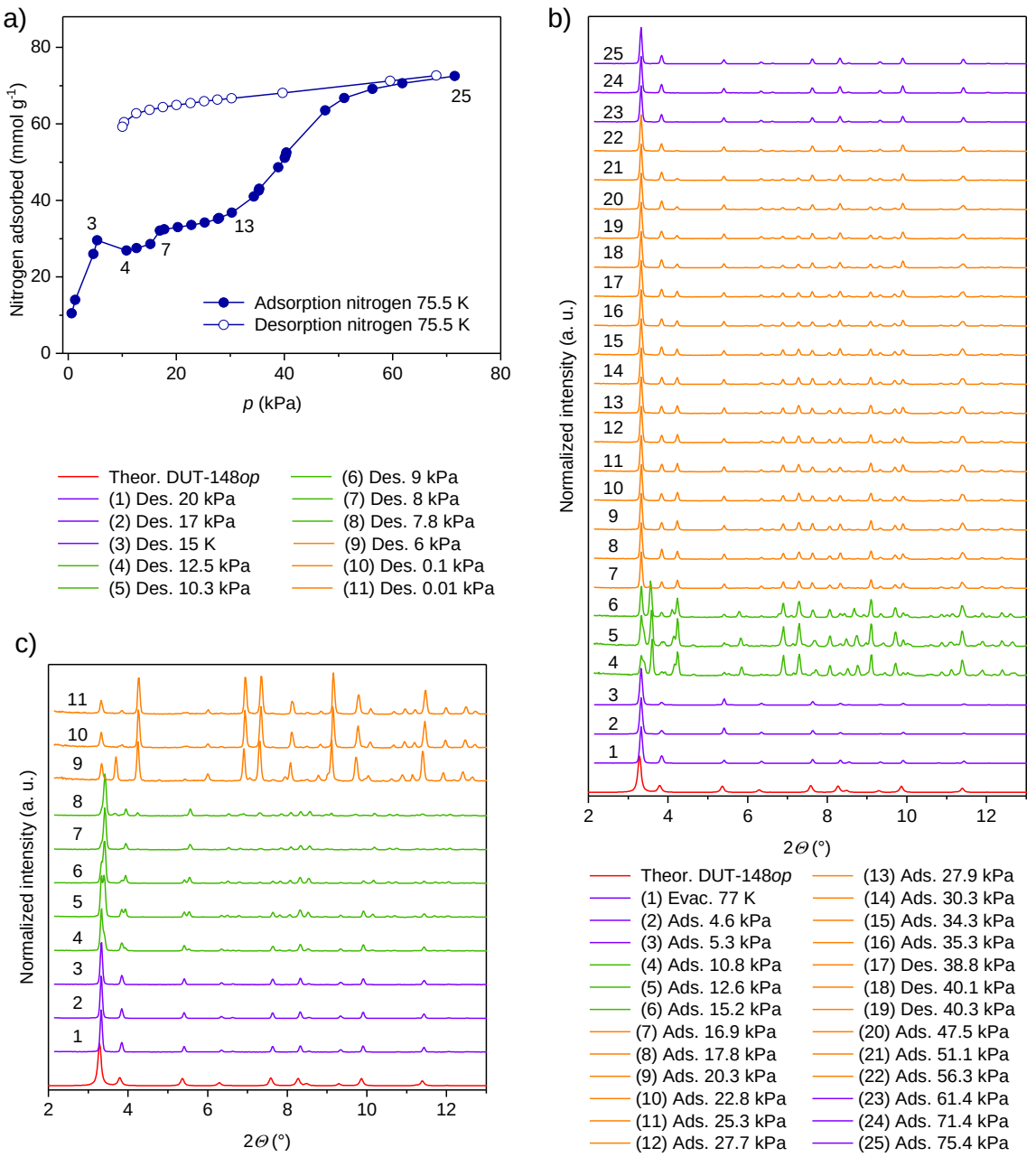

Supplementary Figure 23. *In situ* PXRD in parallel to nitrogen physisorption at 75.5 K of DUT-148: a) Adsorption-desorption isotherm, selected points are labeled by numbers. Filled symbols correspond to adsorption, empty symbols to desorption. b) PXRD pattern recorded during adsorption and c) PXRD pattern recorded during desorption, color code: DUT-148*cp* (orange), DUT-148i*p* (green), DUT-148*op* (purple), and simulated pattern *op* (red)).

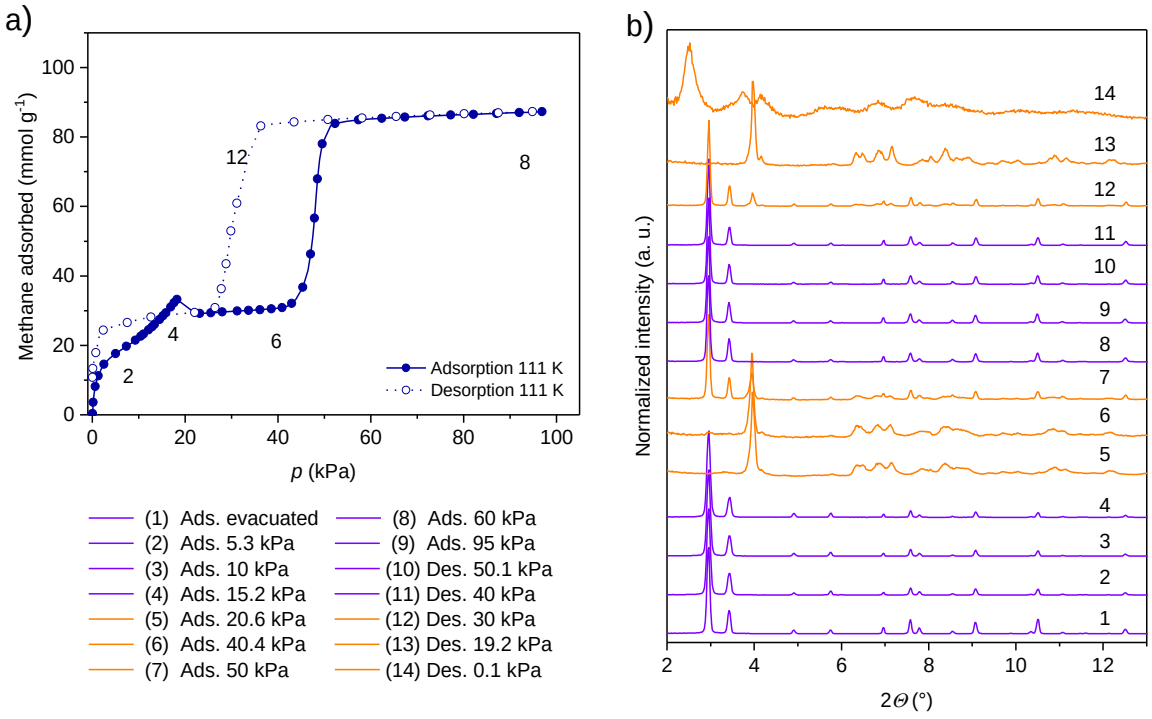

Supplementary Figure 24. *In situ* PXRD in parallel to methane physisorption at 111 K of DUT-160: a) Adsorption-desorption isotherm, selected points are labeled by numbers. Filled symbols correspond to adsorption, empty symbols to desorption. b) PXRD patterns color code: DUT-160*cp* (orange), DUT-160*op* (purple).

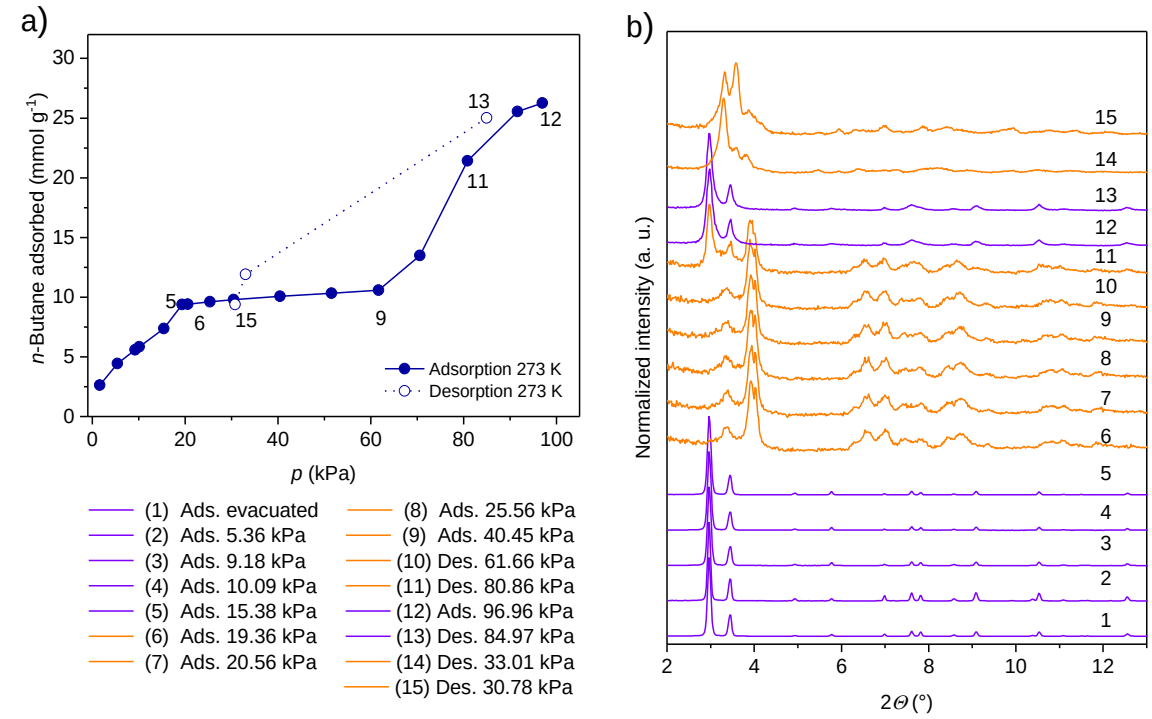

Supplementary Figure 25. *In situ* PXRD in parallel to *n*-butane physisorption at 273 K of DUT-160: a) Adsorption-desorption isotherm, selected points are labeled by numbers. Filled symbols correspond to adsorption, empty symbols to desorption. b) PXRD patterns, color code: DUT-160*cp* (orange), DUT-160*op* (purple).

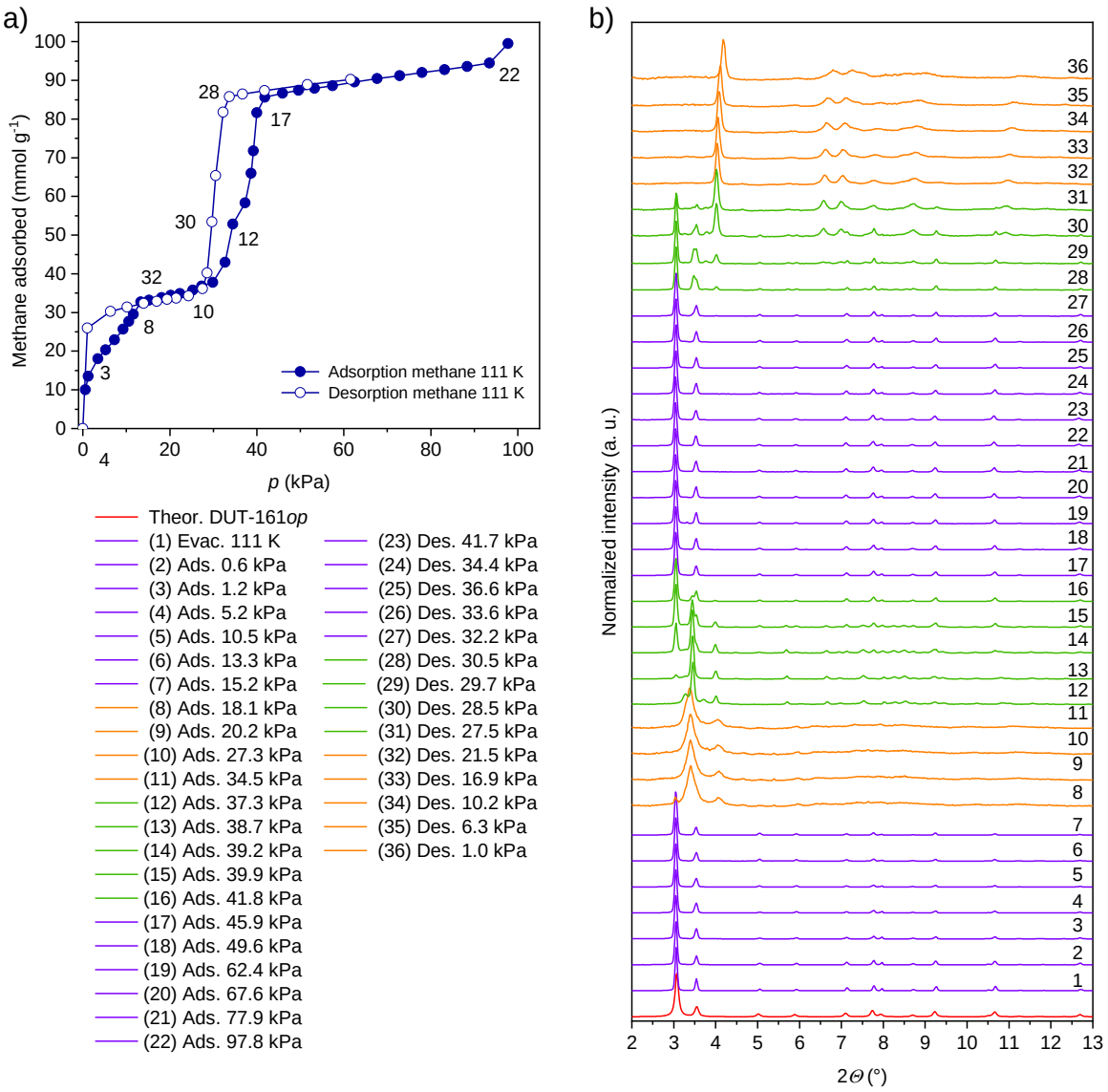

Supplementary Figure 26. *In situ* PXRD in parallel to methane physisorption at 111 K of DUT-161: a) Adsorption-desorption isotherm, selected points are labeled by numbers. Filled symbols correspond to adsorption, empty symbols to desorption. b) PXRD patterns, color code: DUT-160*cp* (orange), DUT-160*op* (purple), mixtures or unidentified intermediate phases (green).

13 Pawley and Rietveld refinement of PXRD data

Refinement of DUT-147*cp* and DUT-148*cp* structures

In situ PXRD patterns, measured during the adsorption of methane at 111 K on DUT-160 and DUT-161, nitrogen at 75.5 K on DUT-148 and *n*-butane at 273 K on DUT-160 and DUT-161 were indexed and profile was refined using Le Bail fit[20], implemented into the FullProf software[21]. The evolution of the unit cell volume during adsorption of fluids on above mentioned MOFs is given in Supplementary Figure 33.

PXRD patterns measured in vacuum on DUT-147, DUT-148, DUT-160, DUT-161 were used for the Rietveld analysis of the desolvated structures. The refinement was performed using the Reflex tool of Materials Studio 5.0. Structural models of corresponding MOFs in artificially reduced symmetry ($Pa\bar{3}$ space group) were used in order to eliminate the disorder. Because of low data / parameter ratio, rigid body refinement was used, in which copper atoms, carboxylates, carbazole moieties and corresponding backbone (pyrene – DUT-147, dihydrophenanthrene – DUT-148, phenyl rings and acetylene group – DUT-160 and phenyl rings + ethylene moiety – DUT-161) were defined as rigid bodies. Rietveld refinement with energy (contribution of UFF ~1%) was used in refinement.

PXRD patterns measured in vacuum at 273 K after *n*-butane physisorption on DUT-147 and PXRD patterns measured after reaching adsorption equilibrium at 40 kPa of *n*-butane at 273 K on DUT-148 were used for Rietveld refinement of the corresponding contracted phases. Structural models in $Pa\bar{3}$ space groups with 6 molecules of *n*-butane per paddle-wheel in the pores were used as initial model. The rigid body Rietveld refinement with energy contribution (UFF ~1%) was performed and both framework and *n*-butane molecules were refined.

Because we could not observe a phase pure *cp* phase of DUT-147 in any of in situ PXRD experiments PXRD patterns measured upon desorption of *n*-butane at p = 1 kPa was used in the Rietveld refinement. This PXRD pattern contains the phase mixture with the highest amount of the *cp* phase (empirically derived from the intensity of the characteristic reflections). The 2Theta range which contains the main reflections of op phase was omitted for refinement because the *cp* phase does not exhibit any reflections in this range as a consequence of the unit cell contraction. However, the characteristic reflections of *op* and *cp* phases, observed at higher 2Thetha angles are found to overlap and cannot be omitted. This leads to an increase of the convergence criteria of the Rietveld refinement and mismatch in intensities, observed in Supplementary Figure 28. Attempts to refine *op* and *cp* phase in parallel did not improve the results.

The Rietveld plots are given in Supplementary Figure 27, Supplementary Figure 32, and experimental data on refinements are summarized in the Supplementary Table 7 and Supplementary Table 8.

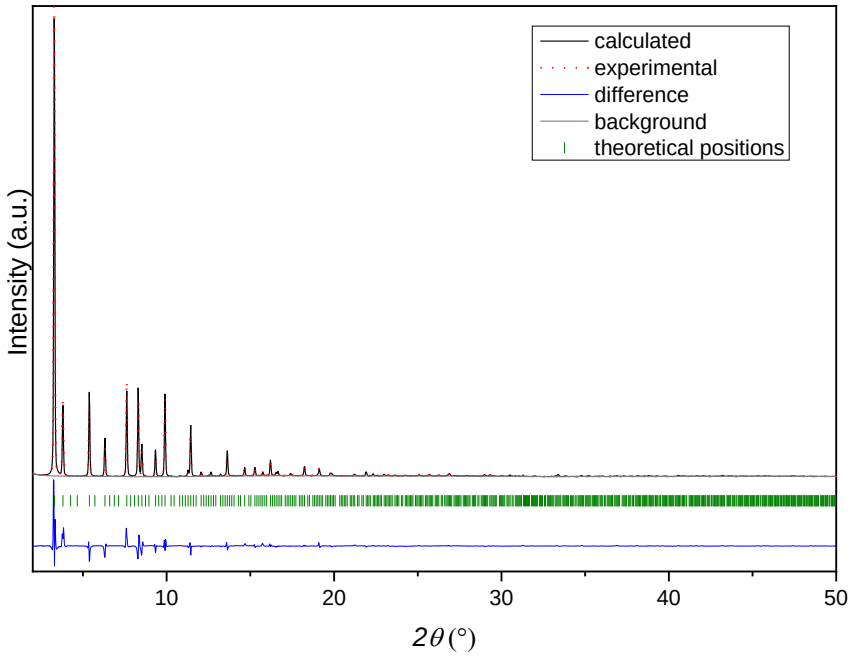

Supplementary Figure 27. Rietveld plot of DUT-147*op* (vacuum 273 K).

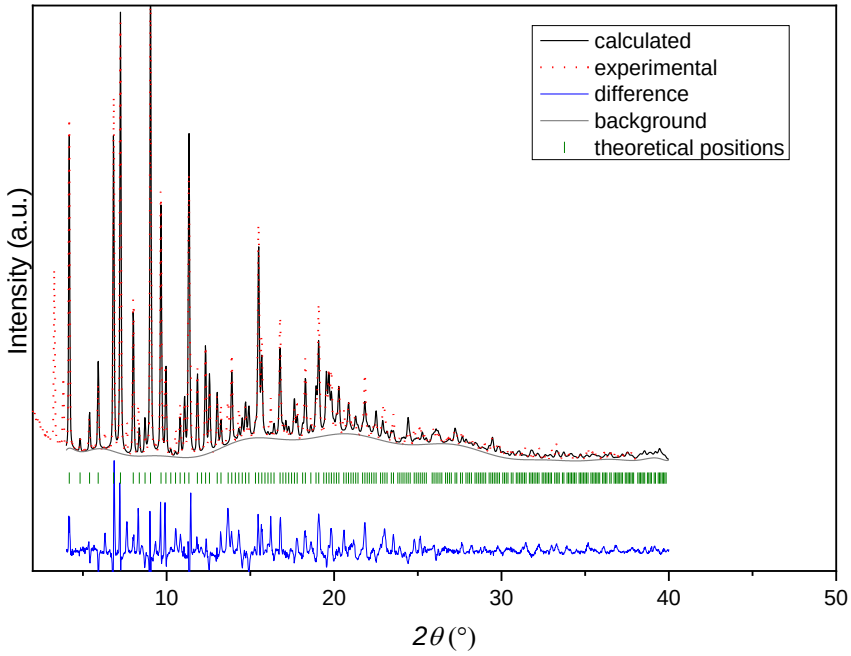

Supplementary Figure 28. Rietveld plot of DUT-147*cp* (desorption <1 kPa *n*-butane 273 K).

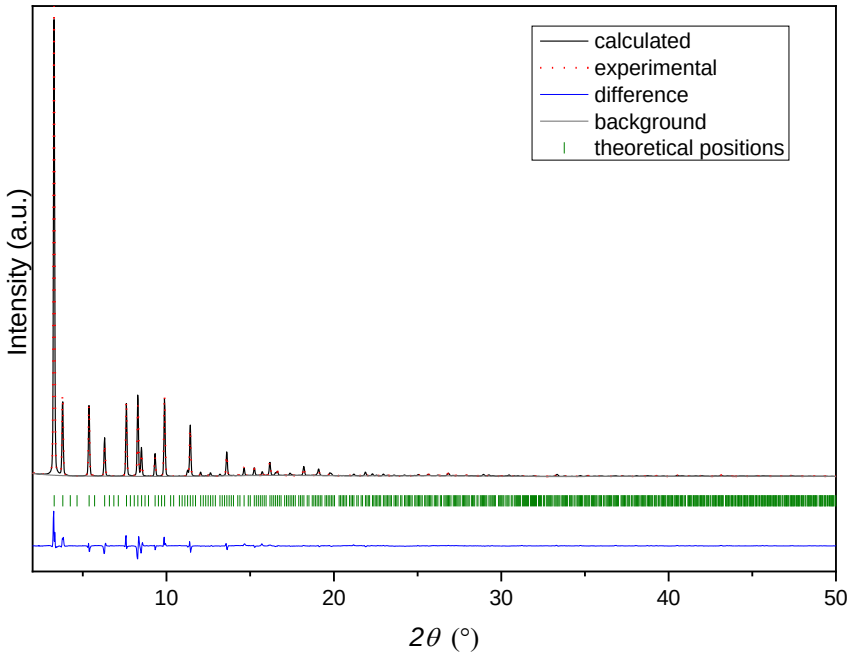

Supplementary Figure 29. Rietveld plot of DUT-148*op* (vacuum 273 K).

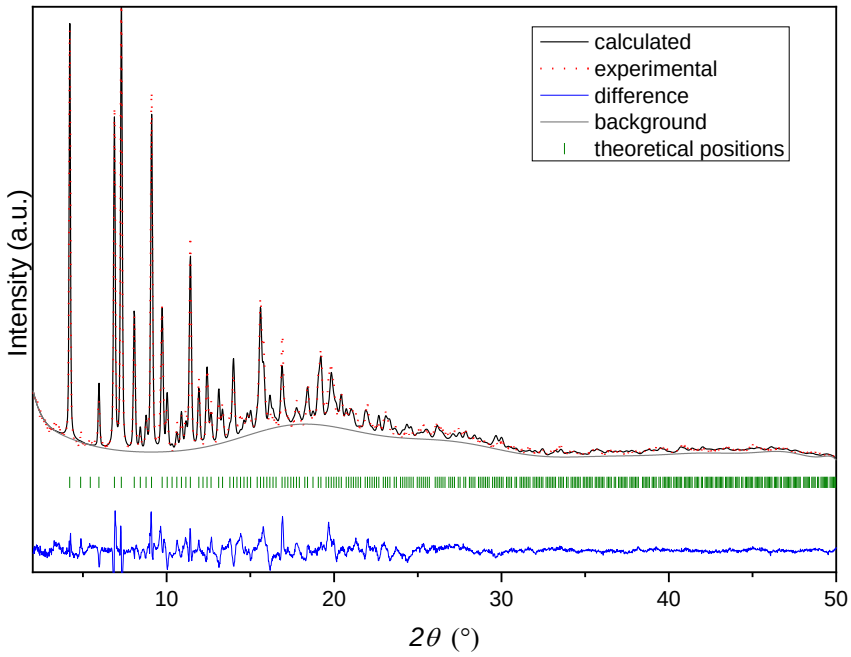

Supplementary Figure 30. Rietveld plot of DUT-148*cp* (adsorption 40 kPa *n*-butane 273 K).

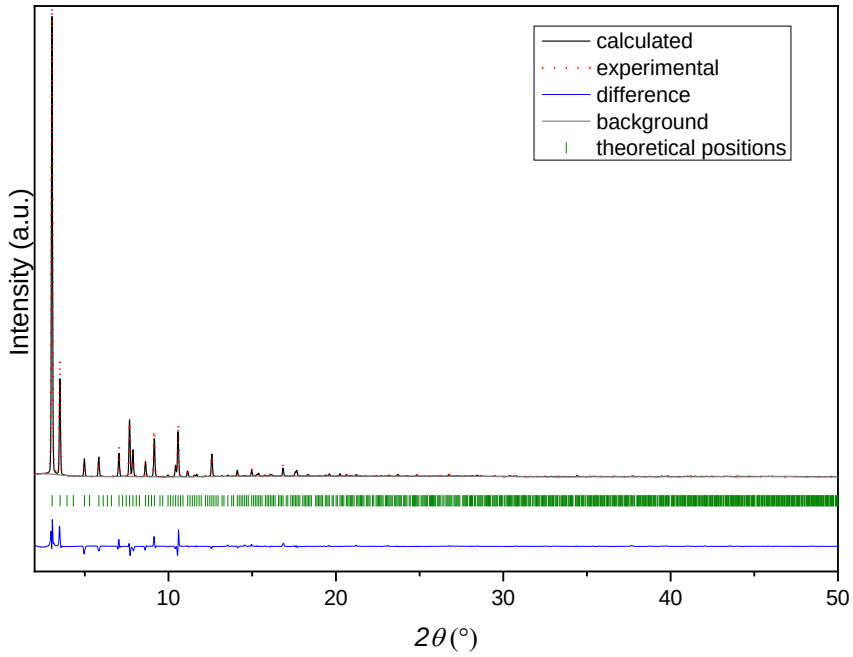

Supplementary Figure 31. Rietveld plot of DUT-160*op* (vacuum 111 K).

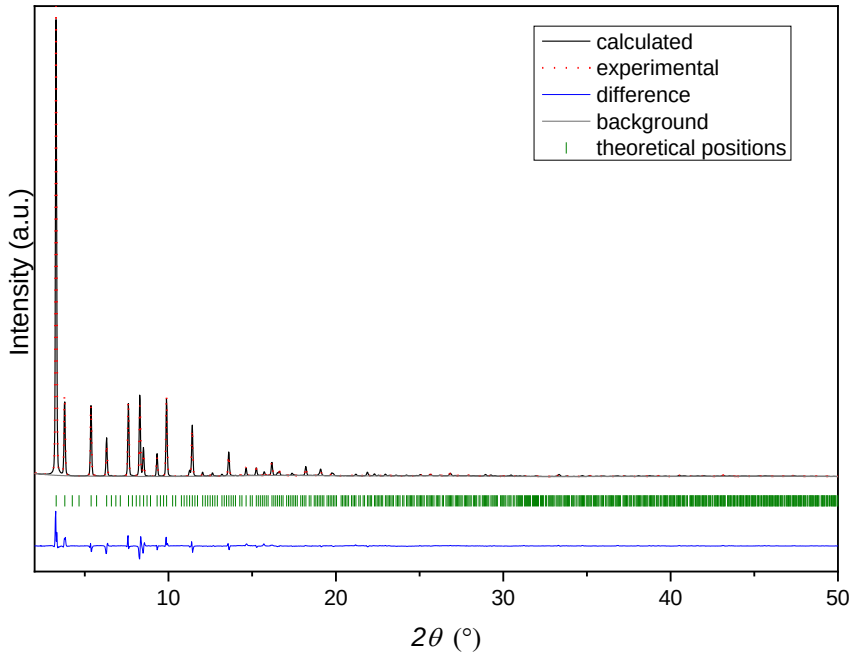

Supplementary Figure 32. Rietveld plot of DUT-161*op* (vacuum 111 K).

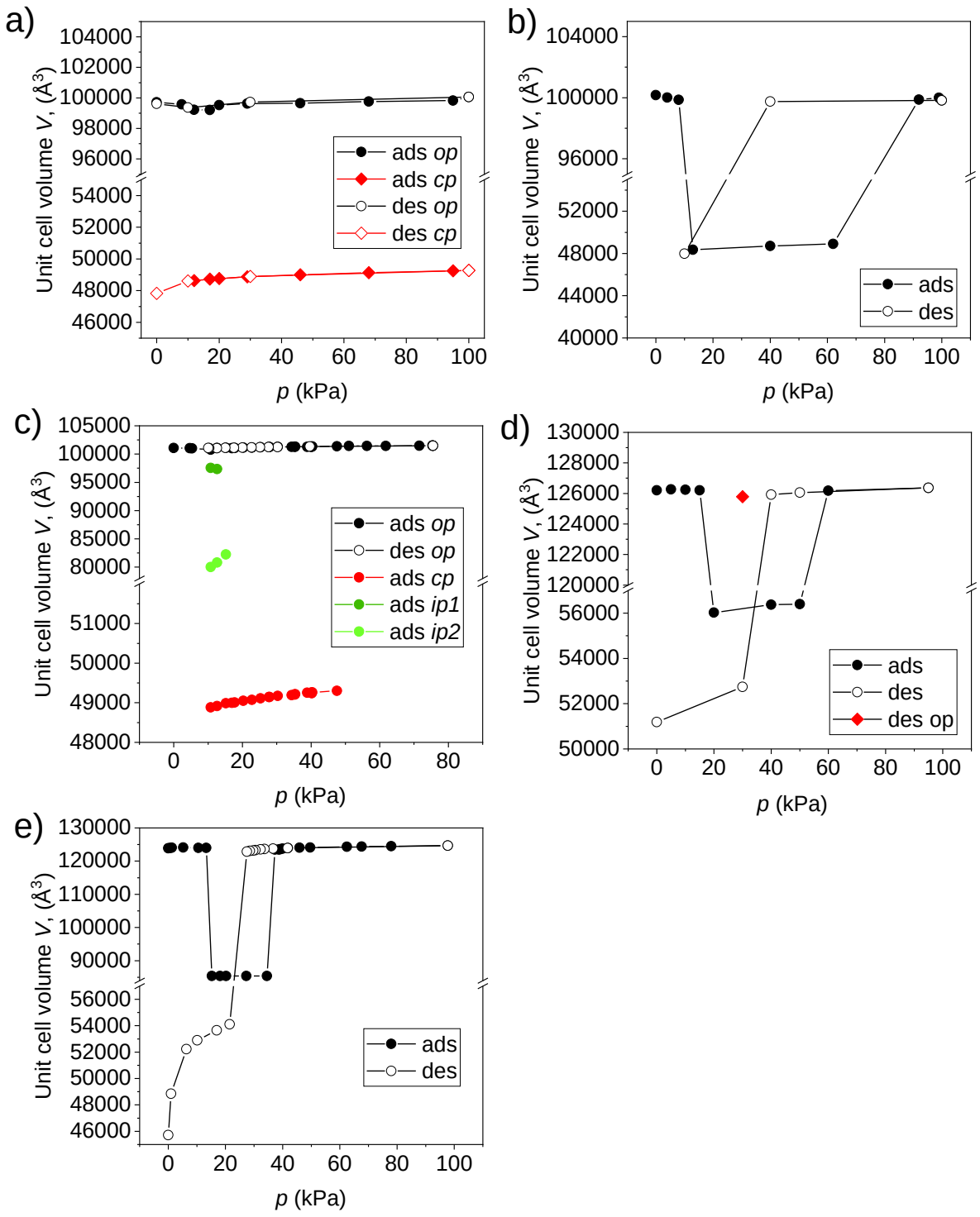

Supplementary Figure 33. Evolution of the unit cell volume upon as adsorption: a) *n*-butane on DUT-147 at 273 K; b) *n*-butane on DUT-148 at 273 K; c) nitrogen on DUT-148 at 75.5 K; d) methane on DUT-160 at 111 K; e) methane on DUT-161 at 111 K.

Supplementary Table 7. Experimental data on Rietveld refinement of DUT-147 and DUT-148 structures.

	DUT-147*op* vacuum 273 K	**DUT-148*op*** vacuum 273 K	**DUT-147*cp*** *n*-butane 273 K	**DUT-148*cp*** *n*-butane 273 K
	Supplementary Figure 27	Supplementary Figure 28	Supplementary Figure 29	Supplementary Figure 30
Formula unit	$C_{44}H_{20}Cu_2N_2O_8$	$C_{42}H_{22}Cu_2N_2O_8$	$C_{44}H_{20}Cu_2N_2O_8 \supset 6C_4H_{10}$	$C_{42}H_{22}Cu_2N_2O_8 \supset 6C_4H_{10}$
Z	24	24	24	24
Symmetry, space group	cubic, $Pa\bar{3}$	cubic, $Pa\bar{3}$	cubic, $Pa\bar{3}$	cubic, $Pa\bar{3}$
Unit cell parameter, *a* (Å)	46.3743 (11)	46.4426(8)	36.5924(15)	36.337
Unit cell volume, (Å^3)	99731.4	100173.0	48997.8	47978.6
Wave length (Å)	1.5406			
2θ range (°)	2 - 50	2 - 50	4 - 40	2 - 50
Instrument geometry	Debye-Scherrer			
Zero point line shift (°)	0	0	0	0
Profile function	Thompson-Cox-Hastings			
U	0.18752	0.25181	0.03173	-0.13854
V	-0.03441	-0.03780	-0.00390	0.14424
W	0.00505	0.00654	0.00408	-0.00040
X	0.03457	-0.00064	0.36644	0.28784
Y	0.02425	0.02095	0.01411	0.03139
Asymmetry correction	Berar-Baldinozzi			
P1	-0.01281	-0.01288	0.00463	0.00653
P2	-0.00010	0.00021	0.00100	0.00013
P3	-0.01092	-0.00589	0.00930	0.00119
P4	-0.00209	-0.00114	0.00164	0.00021
Final R_{wp}	0.1732	0.11187	0.1455	0.0878
Final R_p	0.1328	0.0881	0.1092	0.0675

Supplementary Table 8. Experimental data on Rietveld refinement of DUT-160op and DUT-161op structures.

	DUT-160*op* vacuum 111 K	**DUT-161*op*** vacuum 111 K
	Supplementary Figure 31	Supplementary Figure 32
Formula unit	$C_{42}H_{20}Cu_2N_2O_8$	$C_{42}H_{22}Cu_2N_2O_8$
Z	24	24
Symmetry, space group	cubic, $Pa\bar{3}$	cubic, $Pa\bar{3}$
Unit cell parameter, *a* (Å)	50.1601(2)	49.8406(13)
Unit cell volume, (Å^3)	126200	123809
Wave length (Å)	1.5406	
2θ range (°)	2 - 50	2 - 50
Instrument geometry	Debye-Scherrer	
Zero point line shift (°)	0	0
Profile function	Thompson-Cox-Hastings	
U	0.01559	0.01000
V	-0.01579	-0.01587
W	0.00579	0.00522
X	0.13872	0.27949
Y	0.00587	0.00063
Asymmetry correction	Berar-Baldinozzi	
P1	-0.01626	-0.01263
P2	-0.00055	-0.00009
P3	-0.00419	-0.00090
P4	-0.00056	-0.00018
Final R_{wp}	0.1730	0.1489
Final R_p	0.1207	0.1056

14 Calorimetric analysis of gas adsorption

In situ calorimetric adsorption studies were performed using a protocol previously applied in the characterisation of DUT-49 and related solids.[1, 9] The following description is a literal adaption from reference[1]:

For microcalorimetry, all isotherms and enthalpies were measured experimentally using a Tian-Calvet type microcalorimeter coupled with a home-made manometric gas dosing system[22]. This apparatus allows the simultaneous measurement of the adsorption isotherm and the corresponding differential enthalpies. Gas is introduced into the system using a step-by-step method and each dose is allowed to stabilize in a reference volume before being brought into contact with the adsorbent located in the microcalorimeter. The introduction of the adsorbate to the sample is accompanied by an exothermic thermal signal, measured by the thermopiles of the microcalorimeter. The peak in the calorimetric signal is integrated over time to give the total energy released during this adsorption step. Around 0.05 g of sample is used in each experiment. For each injection of gas, equilibrium was assumed to have been reached after 130 minutes. This was confirmed by the return of the calorimetric signal to its baseline ($< 5\ \mu W$). The gases used for the adsorption experiment were obtained from Air Liquide and were of minimum N47 quality (99.997 % purity).

To obtain the experimental errors, the procedure described in the *Guide to the Expression of Uncertainty in Measurement* was used. The quantity, enthalpy or pressure, is first expressed as a function $f(y)$ of other physical measured quantities. The standard uncertainty ($u_c(y)$) is then calculated on the basis of, where $u_i(x_i)$ is the standard uncertainty in each input quantity. Here it is assumed that the input quantities are independent and uncorrelated. The error margins (a_i) for each quantity were taken from manufacturer specifications of the equipment used for recording. They were then divided by a value k_i chosen to cover the expected variance in that quantity, as each variable is assumed to be characterized by a probability distribution. The error introduced by the equation of state used (NIST REFPROP[23]) were assumed to be minor compared to the error introduced by the physical quantities, with the same to be said regarding the error in the calorimetric heat signal, which represents less than 1% of the error in enthalpy. Finally, the expanded uncertainty was calculated by choosing a suitable coverage factor of 1.645, corresponding to a 95% confidence interval.

$$f(y) = f(N_1, N_2 \ldots N_i) \tag{1}$$

$$u_c(y) = \sqrt{\sum_{i=1}^{N} \left(\frac{\partial f(y)}{\partial x_i} \times u_i(x_i) \right)^2} \tag{2}$$

Supplementary Table 9. Parameters used to estimate the errors of *in situ* calorimetric analysis.

Variable (i)	a_i	k_i
Pressure, *p* (Pa)	20	$\sqrt{3}$
Temperature, *T* (K)	0.1	3
Sample mass, *m* (g)	$1\text{x}10^{-4}$	$\sqrt{3}$
Reference volume, V_r (m^3)	$1\text{x}10^{-9}$	$\sqrt{6}$
Cell volume, V_c (m^3)	$6\text{x}10^{-7}$	$\sqrt{6}$

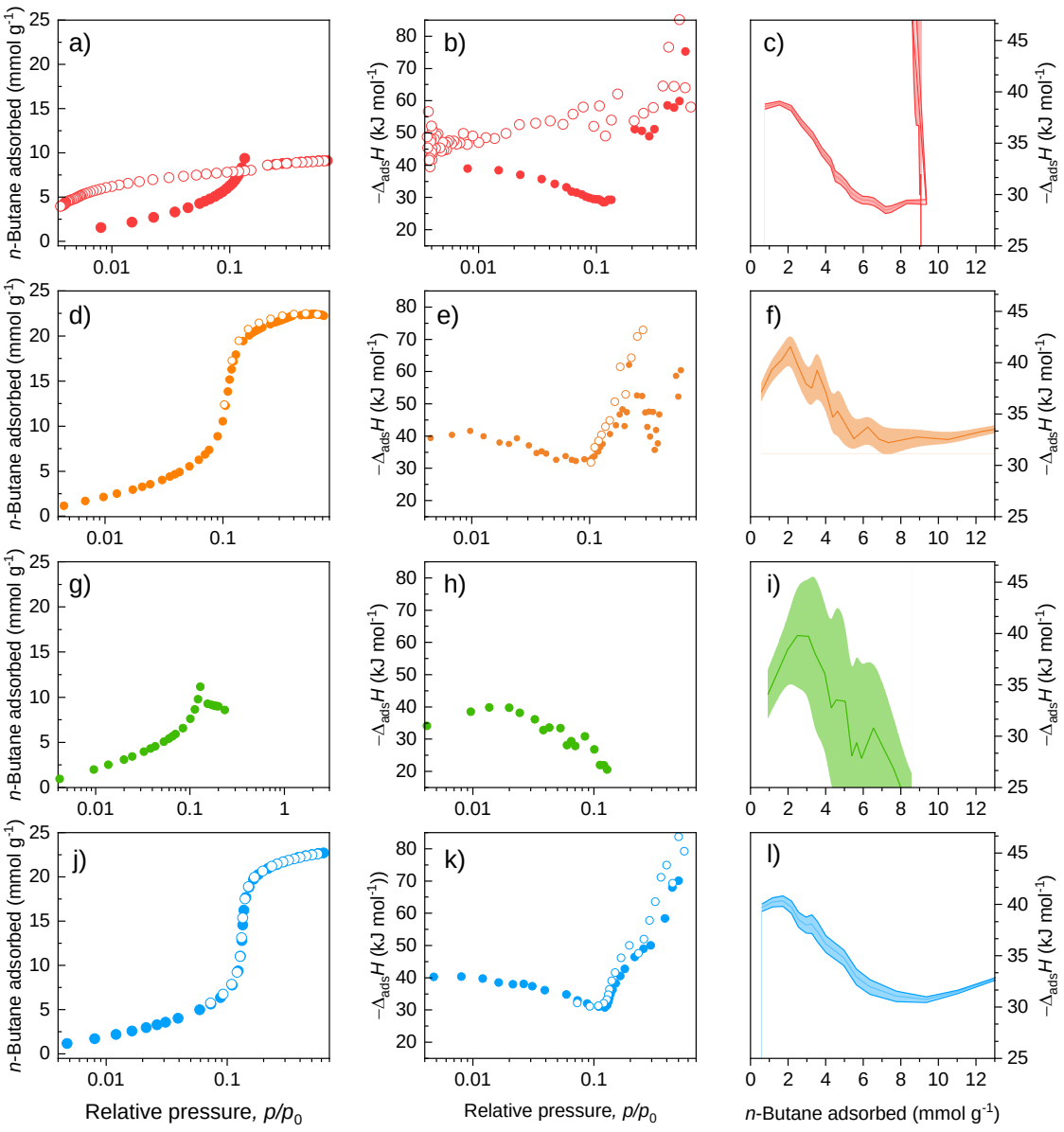

Supplementary Figure 34. Adsorption (filled symbols) and desorption (empty symbols) isotherms of *n*-butane at 303 K (left), corresponding adsorption/desorption enthalpies with error bars (middle), and isosteric adsorption enthalpy profiles with semi-transparent error region (right) of a-c) DUT-49, d-f) DUT-147, g-i) DUT-148, j-l) DUT-160.

15 Computational methods

Adsorption energetics and isotherm simulation

Grand canonical Monte Carlo (GCMC) simulations were carried out at 77 K and 111 K to compute the adsorption isotherms and enthalpies for nitrogen and methane in DUT-49, DUT-50, DUT-147, DUT-148, DUT-160, DUT-161 and DUT-162 for respective *cp* and *op* forms by employing the Complex Adsorption and Diffusion Simulation Suite (CADSS) code.[24] The simulation box was made of 1 conventional unit cell for all DUT phases. The fugacities for methane at a given thermodynamic condition were computed using the Peng–Robinson equation of state. For each state point, 10^8 Monte Carlo steps were used for both equilibration and production runs. The guest/DUT and guest/guest interactions were treated using a van der Waals contribution with a cutoff of 12 Å. The Lennard-Jones (LJ) potential parameters for the atoms of the inorganic and organic parts of the DUT frameworks were derived from the universal force field (UFF)[25] and DREIDING[26] , respectively. 26 Methane was represented by a single LJ site described by the TraPPE force field. [27] Lorentz–Berthelot (LB) combination rules were used to calculate the cross LJ potential parameters.

Supplementary Table 10. LJ potential parameters for adsorbate-adsorbate and adsorbate-DUT-49 interactions used.

	Guest		Framework				
Atoms	N_2	CH_4	C	H	N	O	Cu
σ (Å)	3.31	3.730	3.47	2.85	3.66	3.12	3.30
ϵ/k_B(K)	36.00	148.00	47.86	7.65	38.98	30.20	2.52

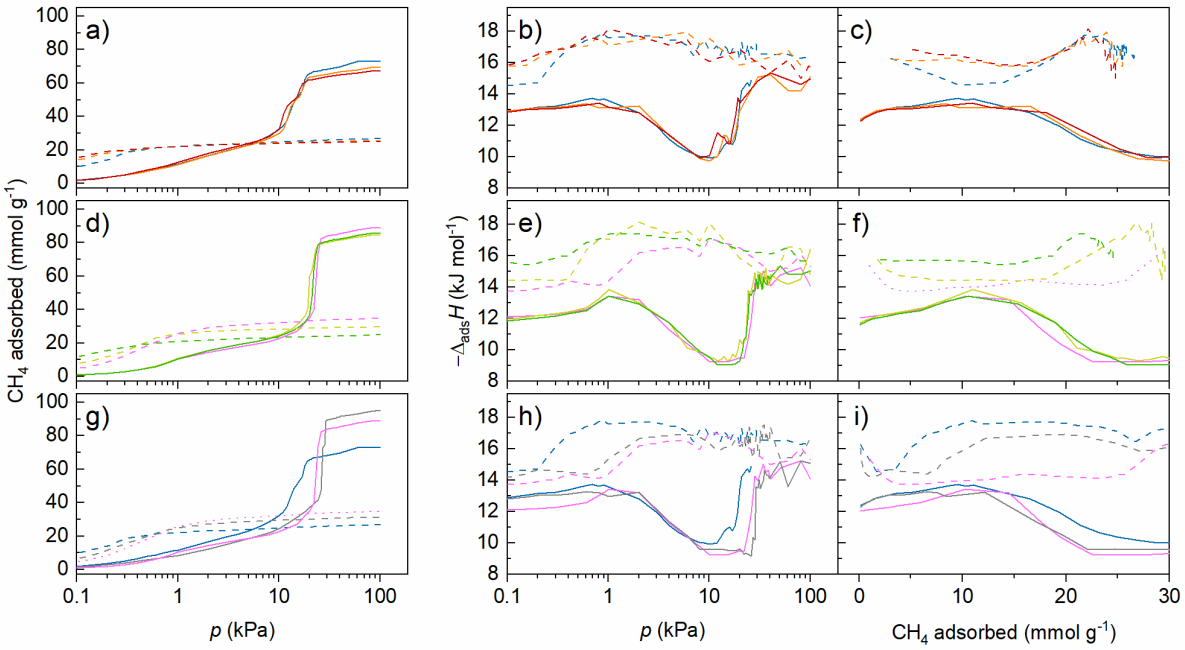

Supplementary Figure 35. a,d,g) Simulated methane adsorption isotherm at 111 K, b,e,h) corresponding simulated adsorption enthalpy profile and c,f,i) corresponding isosteric adsorption enthalpies of DUT-49 (blue), DUT-147 (red), and DUT-148 (orange) (a,b,c), DUT-160 (pink), DUT-161 (yellow), and DUT-162 (green) (d,e,f) and DUT-49, DUT-160, and DUT-50 (grey) (g,h,i). Data for *op* phases in solid and corresponding *cp* phases in dashed lines.

Pore characteristic simulations

Pore characteristics such as density, specific pore volume, and specific accessible surface area were calculated using Zeo++[28]

Supplementary Table 11. Specific surface area, pore volume and density of the series of materials determined by Zeo++ based on simulated crystal structures of *op* and corresponding *cp* phases. Experimental pore volumes were determined from nitrogen adsorption isotherms at 77 K and a relative pressure of 0.95.

Material	Specific geometric surface area simulated ($m^2\ g^{-1}$)	Specific pore volume simulated ($cm^3\ g^{-1}$)	Specific pore volume experimental ($cm^3\ g^{-1}$)	Density ($g\ cm^{-3}$)
49*op*	4950	2.61	2.73	0.321
50*op*	5354	3.59	3.52	0.242
147*op*	4853	2.51	2.68	0.332
148*op*	4995	2.58	2.71	0.323
160*op*	5375	3.38	3.41	0.256
161*op*	5229	3.20	3.19	0.269
162*op*	5342	3.26	1.32	0.263
159*op*	4727	1.53	n. a.	0.500
49*cp*	3324	0.95	n. a.	0.674
50*cp*	3533	1.16	n. a.	0.585
147*cp*	3318	0.93	n. a.	0.686
148*cp*	3331	0.97	n. a.	0.658
160*cp*	3969	1.29	n. a.	0.544
161*cp*	3552	1.10	n. a.	0.607
162*cp*	3242	0.93	n. a.	0.669

Ligand mechanics simulations

Ligand Buckling simulations were performed according to a strategy previously applied on related ligands.[1] The ligands were simulated as the corresponding acids using density functional theory (DFT) simulations employed by the NWCHEM software. The 6-31G+* basis set the hybrid exchange-correlation functional PBE0 were used. Dispersion corrections were included using the Grimme “D3” approach. The optimised structures were subsequently strained by decreasing the N–N length from this local minimum to a compressive strain of 0.06, in 40 steps. For each step, the structure was optimised with default convergence criteria and with this N–N length fixed. Subsequently, a stress-strain curve relative to this axial compression of the ligand is generated; where stress is defined by the gradient of the energy, and strain is the relative decrease in N–N length. The elastic modulus is determined from the gradient in the elastic regime present in the range of low strain values up to the buckling transition.

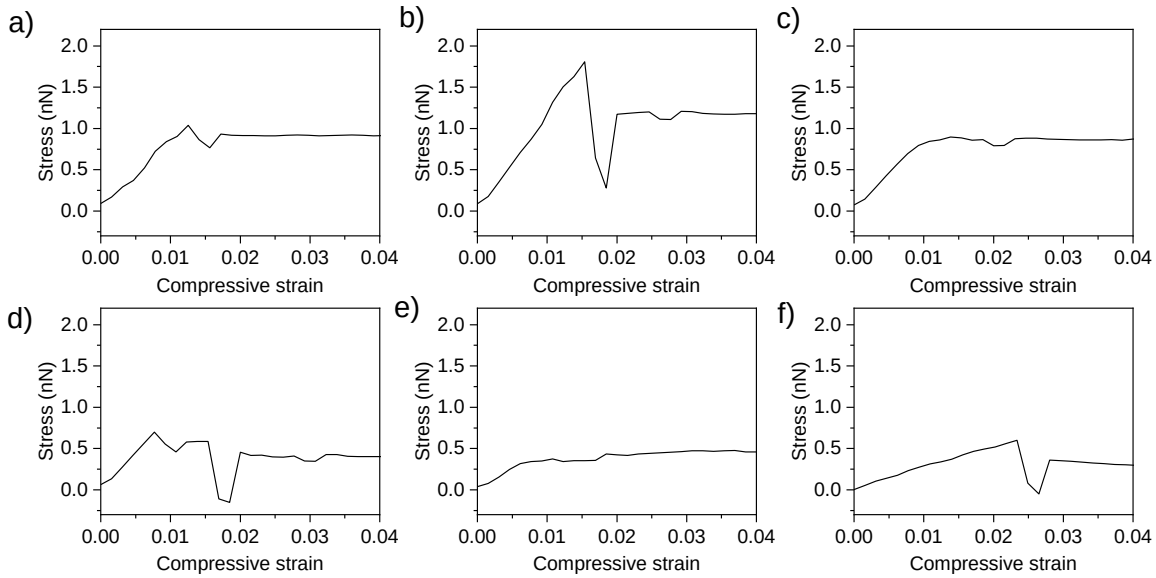

Supplementary Figure 36. Stress-Strain Curves for single ligand buckling for a) L^{49}, b) L^{147}, c) L^{148}, d) L^{160}, e) L^{161}, and f) L^{162}.

Framework dynamics simulations

Molecular dynamics simulations to produce the free energy surfaces relative to different volumes used a modified MOF-FF force field[29] adapted to lammps[30, 31] to describe the bonds, angles, dihedrals and improper dihedrals present in the frameworks. Representative input files for molecular simulations are available online at the data repository https://github.com/jackevansadl/supp-data. The established protocol to compute the pressure-volume equation of states was applied[32], however, a cubic symmetric cell was fixed. The energetic contribution per Ligand can be determined by dividing $\Delta F^{\ddagger}$ with the number of ligands per unit cell which in both the *op* and *cp* phase is 24.

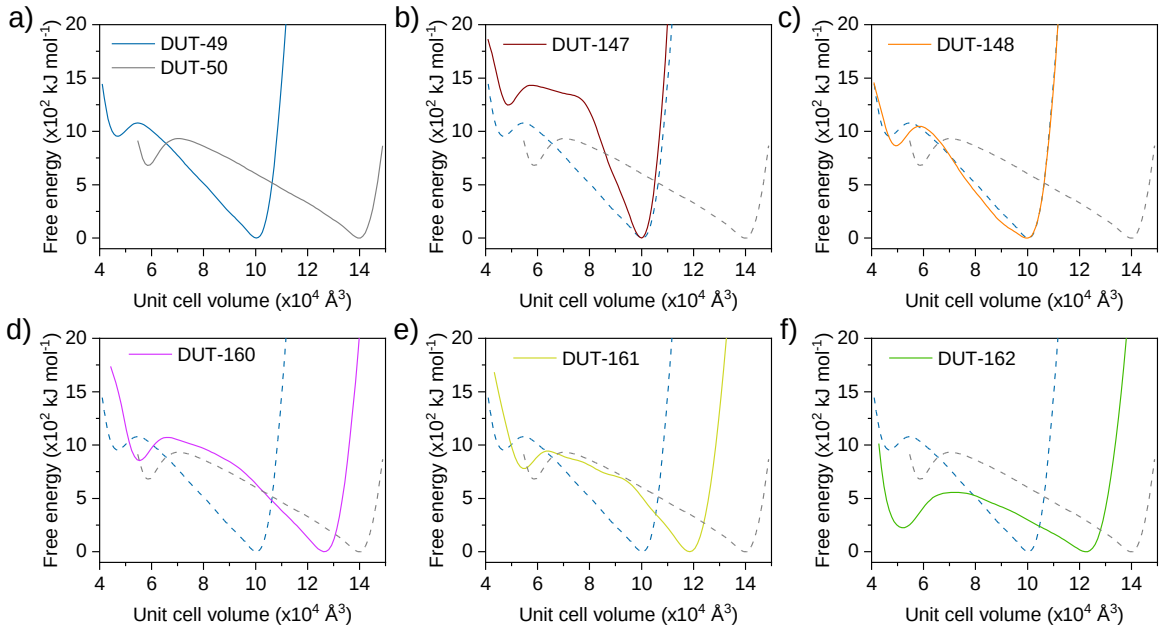

Supplementary Figure 37. Free energy profile of guest free a) DUT-49 and DUT-50, b) DUT-147, c) DUT-148, d) DUT-160, e) DUT-161, and f) DUT-162. In b-f) DUT-49 and DUT-50 are given as dashed lines for reference.

Structural models of the *op* and *cp* phases were generated based on the minima observed in the energy landscapes. Structural models were additionally geometrically optimized which may lead to slight deviations in unit cell volume compared to the actual minimum in the energy surfaces.

Supplementary Table 12. Energy and unit cell parameter derived from free energy profiles and structural models.

Material	ΔF_{op} (kJ mol_{uc}^{-1})	$V_{UC\text{-}op}$ (Å^3)	$\Delta F^{\ddagger}$ (kJ mol_{uc}^{-1})	ΔF_{cp} (kJ mol_{uc}^{-1})	$V_{UC\text{-}cp}$ (Å^3) minimum	$V_{UC\text{-}cp}$ (Å^3) structural model
DUT-49	0	100267	1000	950	47061	46287
DUT-147	0	100004	1420	1240	48453	48300
DUT-148	0	100144	1047	860	49280	48971
DUT-160	0	126118	1071	850	55444	59127
DUT-161	0	118544	942	780	54317	53082
DUT-162	0	1220925	580	220	51686	48339
DUT-50	0	139361	931	670	58478	58557

Throughout the discussion of the manuscript unit cell volumes derived from the structural models of the *cp* phases (CIF of structural model provided as supplementary information) are used.

Supplementary References

1. S. Krause, J. D. Evans, V. Bon, I. Senkovska, P. Iacomi, F. Kolbe, S. Ehrling, E. Troschke, J. Getzschmann, D. M. Többens, A. Franz, D. Wallacher, P. G. Yot, G. Maurin, E. Brunner, P. L. Llewellyn, F.-X. Coudert and S. Kaskel, *Nat. Commun.*, 2019, **10**, 3632.
2. J. Schindelin, I. Arganda-Carreras, E. Frise, V. Kaynig, M. Longair, T. Pietzsch, S. Preibisch, C. Rueden, S. Saalfeld, B. Schmid, J.-Y. Tinevez, D. J. White, V. Hartenstein, K. Eliceiri, P. Tomancak and A. Cardona, *Nat. Methods*, 2012, **9**, 676-682.
3. Ł. J. Weseliński, R. Luebke and M. Eddaoudi, *Synthesis*, 2014, **46**, 596-599.
4. U. Stoeck, I. Senkovska, V. Bon, S. Krause and S. Kaskel, *Chem. Commun.*, 2015, **51**, 1046-1049.
5. W. Lu, D. Yuan, T. A. Makal, Z. Wei, J.-R. Li and H.-C. Zhou, *Dalton Trans.*, 2013, **42**, 1708-1714.
6. S. Krause, V. Bon, H. Du, R. E. Dunin-Borkowski, U. Stoeck, I. Senkovska and S. Kaskel, *Beilstein J. Nanotechnol.*, 2019, **10**, 1737–1744.
7. S. Krause, J. D. Evans, V. Bon, I. Senkovska, F.-X. Coudert, D. M. Többens, D. Wallacher, N. Grimm and S. Kaskel, *Faraday Discuss.*, 2020, DOI: 10.1039/D0FD00013B.
8. S. Krause, V. Bon, I. Senkovska, U. Stoeck, D. Wallacher, D. M. Többens, S. Zander, R. S. Pillai, G. Maurin, F. o.-X. Coudert and S. Kaskel, *Nature*, 2016, **532**, 348-352.
9. S. Krause, J. D. Evans, V. Bon, I. Senkovska, S. Ehrling, U. Stoeck, P. G. Yot, P. Iacomi, P. Llewellyn, G. Maurin, F.-X. Coudert and S. Kaskel, *J. Phys. Chem. C*, 2018, **33**, 19171-19179.
10. S. Henke, M. T. Wharmby, G. Kieslich, I. Hante, A. Schneemann, Y. Wu, D. Daisenberger and A. K. Cheetham, *Chem. Sci.*, 2018, **9**, 1654-1660.
11. U. Mueller, R. Förster, M. Hellmig, F. U. Huschmann, A. Kastner, P. Malecki, S. Pühringer, M. Röwer, K. Sparta, M. Steffien, M. Ühlein, P. Wilk and M. S. Weiss, *EPJ Plus*, 2015, **130**, 141.
12. T. G. G. Battye, L. Kontogiannis, O. Johnson, H. R. Powell and A. G. W. Leslie, *Acta Crystallogr. D*, 2011, **67**, 271-281.
13. K. M. Sparta, M. Krug, U. Heinemann, U. Mueller and M. S. Weiss, *J. Appl. Crystallogr.*, 2016, **49**, 1085-1092.
14. G. Sheldrick, *Acta Crystallogr. C*, 2015, **71**, 3-8.
15. A. Spek, *Acta Crystallogr. C*, 2015, **71**, 9-18.
16. Helmholtz-Zentrum Berlin für Materialien und Energie, *JLSRF*, 2016, **2**, A49.
17. V. Bon, I. Senkovska, D. Wallacher, A. Heerwig, N. Klein, I. Zizak, R. Feyerherm, E. Dudzik and S. Kaskel, *Microporous Mesoporous Mater.*, 2014, **188**, 190-195.
18. P. A. Heiney, *Datasqueeze 2.2.9 Graphical Tool for X-ray Data Analysis*, 2012.

19. M. Wojdyr, *J. Appl. Crystallogr.*, 2010, **43**, 1126-1128.
20. A. L. Bail, *Powder Diffr.*, 2005, **4**, 316-326.
21. J. Rodriguez-Carvajal, *Journal*, 2006.
22. P. L. Llewellyn and G. Maurin, *C. R. Chim.*, 2004, **8**, 283-302.
23. I. H. B. Eric W. Lemmon, Marcia L. Huber, and Mark O. McLinden, *Journal*, 2018, **10**.
24. Q. Yang and C. Zhong, *J. Phys. Chem. B*, 2006, **110**, 17776-17783.
25. A. K. Rappe, C. J. Casewit, K. S. Colwell, W. A. Goddard and W. M. Skiff, *J. Am. Chem. Soc.*, 1992, **114**, 10024-10035.
26. S. L. Mayo, B. D. Olafson and W. A. Goddard, *J. Phys. Chem.*, 1990, **94**, 8897-8909.
27. M. G. Martin and J. I. Siepmann, *J. Phys. Chem. B*, 1998, **102**, 2569-2577.
28. T. F. Willems, C. H. Rycroft, M. Kazi, J. C. Meza and M. Haranczyk, *Microporous Mesoporous Mater.*, 2012, **149**, 134-141.
29. S. Bureekaew, S. Amirjalayer, M. Tafipolsky, C. Spickermann, T. K. Roy and R. Schmid, *Phys. Status Solidi B*, 2013, **250**, 1128-1141.
30. S. Plimpton, *J. Comput. Phys.*, 1995, **117**, 1-19.
31. P. G. Boyd, S. M. Moosavi, M. Witman and B. Smit, *J. Phys. Chem. Lett.*, 2017, **8**, 357-363.
32. S. M. J. Rogge, M. Waroquier and V. Van Speybroeck, *Acc. Chem. Res.*, 2018, **51**, 138-148.